Theory of Multimode Laser Operation*

C. L. O'Bryan, III† and M. Sargent, III
Optical Sciences Center, University of Arizona, Tucson, Arizona 85721
(Received 25 June 1973)

The Lamb semiclassical laser theory is developed uniformly for multimode unidirectional ring, two-mirror, and bidirectional-ring lasers. Equations are given which determine the mode amplitudes and frequencies to third order in the electric-dipole interaction energy. A diagram technique called the perturbation tree is used to bypass most of the algebra for the complicated multimode bidirectional-ring case. Numerical results are given for a variety of multimode laser configurations in the free-run approximation. In particular it is shown that the multimode, two-mirror gas laser exhibits an asymmetric spectrum in agreement with the experimental observations of Garside. This asymmetry is found to be absent in the unidirectional-ring case and is attributed to mode competition for the same pairs of velocity ensembles (an origin related to that for the Lamb dip). The coupling role of population pulsations is discussed with numerical illustrations. Treatment of mode locking is deferred to a forthcoming companion paper.

I. INTRODUCTION

Semiclassical perturbation theory has proved to be particularly effective in the analysis of laser operation. The original theory of Lamb[1] is based on a self-consistent field approach; that is, the field assumed to induce the polarization of the active medium is set equal to the field produced by this polarization. The classical field is governed by Maxwell's equations, while the atomic medium is treated quantum mechanically. Lamb's paper predicted threshold and linear pulling and gave insight into a variety of effects such as hole burning,[2] population pulsations,[1] and frequency-pushing phenomena. In particular, the theory predicted a dip in intensity of a single-mode standing-wave laser as the resonator is tuned through the center of the atomic line ("Lamb dip"); it described mode competition effects in the two-mode laser and beat frequency locking in a three-mode laser. A theoretical approach to laser operation similar to Lamb's has been given by Haken and Sauermann.[3]

The theory has subsequently been extended in many directions. For example, the case of a ring laser with two oppositely directed traveling waves was investigated.[4] The general Zeeman laser was solved[5] for an arbitrarily oriented magnetic field, a vector electric field, and cavity anisotropy. In this treatment the two-level atomic system was generalized to include isotopes, arbitrary angular momenta, and hyperfine structure. The third-order theory has been extended to fifth order in the perturbation energy for a single-mode standing-wave laser.[6] A fully quantized generalization was developed[7] in order to treat the laser linewidth and buildup from vacuum. Effects of collisions in the atomic medium have been investigated.[8] More recently, the single-mode semiclassical theory has been extended to arbitrary intensity for both the standing wave[9] and ring lasers.[10] A review of these laser theories has been given by Sargent and Scully.[11]

None of the previous work has investigated in detail the operation of either normal or ring lasers with more than three modes. Because of the complexity of the analysis the discussion of even the three-mode standing-wave laser has been largely qualitative, except for specific cases presented by Sayers and Allen.[12] The present paper presents the Lamb theory in a computer-oriented version similar to that of Sargent, Fork, and Lamb[5] with additional simplifying techniques such as use of the population matrix $\rho(z, v, t)$, a partial fraction evaluation of the third-order integrals, and a diagrammatic device called a "perturbation tree." This device enables us to write the third-order polarization components with considerably less algebra than in previous developments. Furthermore, we can derive the general amplitude- and frequency-determining equations for multimode operation of unidirectional-ring, two-mirror, *and* bidirectional-ring lasers in a unified fashion. These equations for the bidirectional-ring laser are given here for the first time.[13] Atomic collisions are partially treated by a phenomenological increase in the polarization decay constant. Inasmuch as the theory is carried only to third order in the atom field interaction, application is limited to low intensities. Nevertheless, a simple criterion reveals that many cases of multimode operation can be adequately described and, in particular, the theory agrees with experimental observations of Garside.[14]

In Sec. II we derive from Maxwell's equations the field self-consistency equations relating oscillation amplitudes and frequencies to the induced polarization of the active medium. In Sec. III the

polarization is evaluated for an arbitrary interaction energy. We then specialize this energy to yield polarizations for the unidirectional-ring and two-mirror lasers in Sec. IV, and for the general bidirectional-ring laser in Sec. V. We discuss the free-run approximation (neglect of all terms whose relative phases are not identically zero) in Sec. VI and present an algorithm for finding steady-state multimode intensities. In the remainder of the paper we examine various cases of interest. The two-mode cases can be solved analytically and are used to illustrate physical mechanisms responsible for mode interactions (Sec. VII). We consider lasers with up to ten modes in Sec. VIII. Here we give results of computer "experiments" which show the effects of variations in several laser parameters. We compare the free-run intensities to those obtained from rate equations in which population pulsations are neglected. We also vary the placement of the medium in the cavity, the cavity quality factor Q, and other physical parameters. Finally we compare the results with experiments. A subsequent paper will treat further solutions in which all slowly varying phase angles are retained. These solutions include mode-locked operation. We refer the reader to the review article of Smith[15] for other references of multimode mode-locked operation.

II. ELECTROMAGNETIC FIELD EQUATIONS

In this section we derive self-consistency equations relating the field Fourier amplitudes, frequencies, and phases to corresponding components of the induced polarization. The analysis provides for multimode-ring (as well as two-mirror) laser operation.

The wave equation obtained from Maxwell's equation in an inertial frame for the scalar electric field $E(s,t)$ is

$$\frac{\partial^2 E(s,t)}{\partial s^2} - \mu_0\sigma\frac{\partial E}{\partial t} - \mu_0\epsilon_0\frac{\partial^2 E}{\partial t^2} = \mu_0\frac{\partial^2 P(s,t)}{\partial t^2}, \quad (1)$$

where s is the direction along the optical path of the laser (see Fig. 1). The medium is assumed to be dilute, and the electric field is linearly polarized perpendicular to the axis of the laser structure. Transverse variations of the field are neglected. The cavity losses are represented by a fictional ohmic current $\vec{J} = \sigma\vec{E}$.

We express the electric field as a sum of modes,

$$E(s,t) = \tfrac{1}{2}\sum_n E_n(t)\exp\{-i[\nu_n t + \phi_n(t)]\}U_n(s) + \text{c.c.}, \quad (2)$$

where the amplitudes $E_n(t)$ and phases $\phi_n(t)$ are real slowly varying functions of time and $U_n(s)$ are (possibly complex) normal-mode functions of the laser cavity having the highest Q, namely, those corresponding to the TEM_{00n} longitudinal modes. The functions considered here are real standing waves for the two-mirror laser [Fig. 1(a)] and complex traveling waves for the ring laser. For traveling-wave modes, the mode index n is negative for modes traveling in the negative s direction. The wave number of mode n is given by K_n defined, along with the mode function, by

$$U_n(s) = e^{iK_n s}, \quad K_n = n\pi/L \quad (3)$$

for the bidirectional ring, where L is the round-trip cavity length. For the unidirectional ring, only positive values of n are considered. Modes have no directional dependence for the two-mirror lasers, so again only positive values of n are necessary, and

$$U_n(s) = \sin(K_n s), \quad K_n = n\pi/L \quad (4)$$

where now L is the distance between the laser mirrors.

Similarly, we write the polarization in the form

$$P(s,t) = \tfrac{1}{2}\sum_n \mathcal{P}_n(t)\exp[-i(\nu_n t + \phi_n)]U_n(s) + \text{c.c.}, \quad (5)$$

where $\mathcal{P}_n(t)$ is a complex slowly varying function of time which will be referred to as a complex polarization.

We obtain the self-consistency equations for the field amplitudes and phases by substituting (2) and (5) into (1) and projecting onto $U_n(s)$—that is,

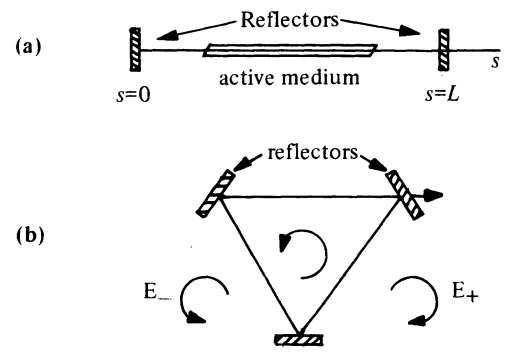

FIG. 1. (a) Diagram of two-mirror laser showing reflectors in plane perpendicular to the laser (s) axis and active medium between the reflectors. Brewster windows are sketched on the ends of the active medium to help enforce the condition that only one polarization component of the electric field exists, as assumed in this paper. (b) Corresponding ring-laser configuration. Usually both running waves oscillate in a ring laser; the unidirectional situation can be achieved by insertion of a device with high loss for one running wave in the cavity.

operating on the equation by $\int_0^L ds\, U_n^*(s)$. We neglect small terms containing $\ddot{E}_n$, $\ddot{\phi}_n$, $\dot{\phi}_n E_n$, $\sigma\dot{\phi}_n$, and $\sigma\dot{E}_n$, since the coefficients are slowly varying and the losses are also small. The polarization components are nearly monochromatic, so that

$$\frac{\partial^2}{\partial t^2}\{\mathcal{P}_n(t)\exp[-i(\nu_n t+\phi_n)]\} \cong -\nu_n^2\mathcal{P}_n(t)\exp[-i(\nu_n t+\phi_n)]. \quad (6)$$

We can treat the optical carriers $e^{-i\nu_n t}$ and $e^{+i\nu_n t}$ as orthogonal components and equate their coefficients separately to zero. We will therefore concentrate on the coefficients of the positive-frequency term $\exp[-i(\nu_n t+\phi_n)]$. The operating frequency of the laser is close to the cavity resonance frequency, so

$$\Omega_n^2-(\nu_n+\dot{\phi}_n)^2\approx 2\nu_n(\Omega_n-\nu_n-\phi_n). \quad (7)$$

Setting $\sigma=\epsilon_0\nu/Q$ to yield the desired Q of the nth mode and equating the real and imaginary parts of the coefficients separately, we find the amplitude- and frequency-determining equations

$$\begin{aligned}\dot{E}_n+\tfrac{1}{2}(\nu_n/Q_n)E_n&=-\tfrac{1}{2}(\nu_n/\epsilon_0)\,\mathrm{Im}(\mathcal{P}_n),\\ \nu_n+\dot{\phi}_n&=\Omega_n-\tfrac{1}{2}(\nu_n/\epsilon_0)E_n^{-1}\,\mathrm{Re}(\mathcal{P}_n).\end{aligned} \quad (8)$$

The E_n equation leads to conservation of energy and the ν_n equation expresses a (real) index of refraction (see Ref. 11 for discussion).

For a rotating ring laser, we should in general consider Maxwell's equations in a noninertial frame, which might require general relativity theory. However, for small rotation rates, Lorentz transformations give similar results. Further, Menegozzi and Lamb[4] have shown that the only effect of laser rotation on the amplitude and frequency equations (8) is a shift in the empty-cavity resonance frequencies $\Omega_n=|K_n|c$ by $2A\dot{\theta}\Omega_n/Lc$, where A is the area enclosed by the laser path and $\dot{\theta}$ is the laser rotation rate. Traveling-wave modes are up or down shifted by this amount, depending on whether they are going in the opposite or same direction as the cavity rotation. It is also possible to achieve frequency splitting between oppositely directed running waves using magneto-optic devices.[16] We denote such a nonreciprocal frequency shift by κ, for which

$$\Omega_n=\Omega_n+\kappa\,\mathrm{sgn}(K_n)$$

is the cavity resonance frequency of a traveling-wave mode.

With this understanding, (8) determines the field amplitudes and frequencies for either a ring or normal standing-wave laser, once the $\mathcal{P}_n(t)$ are known in terms of the $E_n(t)$. To evaluate $\mathcal{P}_n(t)$, we turn to a quantum description of the atomic medium.

III. POLARIZATION OF MEDIUM

We assume the laser medium consists of independent two-level atoms, as depicted in Fig. 2. The atoms are excited to either the upper state a or the lower state b at random positions s and times t. Decay from levels a and b proceeds with spontaneous lifetimes γ_a^{-1} and γ_b^{-1}, respectively. In the absence of collisions, an atom with axial velocity v moves such that at time t its position is

$$s=s_0+v(t-t_0). \quad (9)$$

When the atom is in the presence of an electric field, it experiences a perturbation interaction with energy

$$\mathcal{V}_{ab}(s,t)=-\wp E(s,t), \quad (10)$$

where $\wp$ is the real matrix element for the electric-dipole moment of the atom.

The density matrix $\rho(\alpha, s_0, t_0, v, t)$ for one atom excited to the α state at time t_0 and position s_0 with velocity v obeys the equation of motion

$$\dot{\rho}=(-i/\hbar)[\mathcal{H},\rho]-\tfrac{1}{2}(\Gamma\rho+\rho\Gamma), \quad (11)$$

with

$$\mathcal{H}=\begin{pmatrix}\hbar\omega_a & \mathcal{V}_{ab}\\ \mathcal{V}_{ba} & \hbar\omega_b\end{pmatrix}$$

and

$$\Gamma=\begin{pmatrix}\gamma_a & 0\\ 0 & \gamma_b\end{pmatrix}.$$

The average electric-dipole moment corresponding to this density matrix is

$$\langle p\rangle=\mathrm{Tr}(e\rho r)=\wp\rho_{ab}+\mathrm{c.c.} \quad (12)$$

To find the macroscopic polarization $P(s,t)$, we combine all the microscopic dipoles contributed by atoms excited into either state a or b at any time and location which arrive at s at time t. Thus

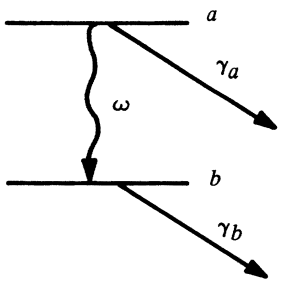

FIG. 2. Level diagram for quantum systems comprising the active medium. In addition to the level decay constants γ_a and γ_b, the dipole-moment term ρ_{ab} decays with the constant γ.

$$P(s,t) = \wp \int_{-\infty}^{\infty} dv \sum_{\alpha=a,b} \int_{-\infty}^{t} dt_0 \int ds_0 \lambda_\alpha(s_0, v, t_0) \times \rho_{ab}(\alpha, s_0, t_0, v, t) \delta(s - s_0 - vt + vt_0) + \text{c.c.}, \tag{13}$$

where $\lambda_\alpha(s_0, v, t_0)$ is the number of atoms excited to state α at time t_0, position s_0, with axial velocity v. It is convenient to integrate the density matrix over the excitation time t_0, places s_0, and states α before integrating (11). This results in the population matrix

$$\rho(s,v,t) = \sum_{\alpha=a,b} \int_{-\infty}^{t} dt_0 \lambda_\alpha(s,v,t_0) \rho(\alpha, s, t_0, v, t), \tag{14}$$

in terms of which the macroscopic polarization is given by

$$P(s,t) = \wp \int_{-\infty}^{\infty} dv \, \rho_{ab}(s,v,t) + \text{c.c.} \tag{15}$$

Combining (5) and (15), we find the complex polarization

$$\mathcal{P}_n(t) = 2\mathfrak{N}^{-1} \exp[i(\nu_n t + \phi_n)] \int_{-\infty}^{\infty} dv \times \int_0^L ds \, U_n^*(s) \wp \rho_{ab}(s,v,t), \tag{16}$$

where the normalization factor is

$$\mathfrak{N} = \int_0^L ds \, |U_n(s)|^2 .$$

Only the slowly varying contribution to $\mathcal{P}_n(t)$ is retained in (16). The complex conjugate terms have been neglected, since they oscillate at optical frequencies in time.

The population matrix (14) obeys an equation similar to that (11) for the pure case, namely,

$$\dot{\rho} = \lambda - (i/\hbar)[\mathcal{H}, \rho] - \tfrac{1}{2}(\Gamma\rho + \rho\Gamma), \tag{17}$$

where λ is the matrix of excitation rates

$$\lambda = \begin{pmatrix} \lambda_a & 0 \\ 0 & \lambda_b \end{pmatrix}.$$

The time derivative in (17) is given by

$$\frac{d}{dt} = \frac{\partial}{\partial t} + v \frac{\partial}{\partial s},$$

which appears to result in a partial differential equation. However, it is ordinary, for an equation of the form

$$\left(\frac{\partial}{\partial t} + v \frac{\partial}{\partial s}\right) f(s,v,t) = g(s,v,t)$$

has the formal integral

$$f(s,v,t) = \int_{-\infty}^{t} dt' \, g(s', v, t'),$$

where $s' = s - v(t - t')$ is the position at the earlier time t'. Accordingly, in the perturbation elements $\mathcal{V}_{ab}$ to follow, we take the s dependence to be that at the times indicated, e.g., $\mathcal{V}_{ab}(t')$ has $s' = s - v \times (t - t')$, $\mathcal{V}_{ab}(t''')$ has $s''' = s - v(t - t''')$, etc. The equation of motion (17) for the population matrix has components

$$\begin{aligned} \dot{\rho}_{aa} &= \lambda_a - \gamma_a \rho_{aa} - [(i/\hbar)\mathcal{V}_{ab}(s,t)\rho_{ba}(s,v,t) + \text{c.c.}], \\ \dot{\rho}_{bb} &= \lambda_b - \gamma_b \rho_{bb} + [(i/\hbar)\mathcal{V}_{ab}(s,t)\rho_{ba}(s,v,t) + \text{c.c.}], \\ \dot{\rho}_{ab} &= -(i\omega + \gamma)\rho_{ab} + (i/\hbar)\mathcal{V}_{ab}(s,t)[\rho_{aa} - \rho_{bb}], \\ \rho_{ba} &= \rho_{ab}^*, \end{aligned} \tag{18}$$

where $\omega = \omega_a - \omega_b$. Here we take the decay constant of the off-diagonal elements to be

$$\gamma = \tfrac{1}{2}(\gamma_a + \gamma_b) + \gamma_{\text{phase}} = \gamma_{ab} + \gamma_{\text{phase}}, \tag{19}$$

in which the additional term γ_{phase} results from consideration of interactions which cause slight shifts in the energy levels but not changes of state. These interactions cause small random shifts in the phase of the radiating atomic dipole, effectively terminating its coherent contribution to the field. Hence the decay constant for ρ_{ab} is increased without much change in γ_a or γ_b. The ensemble average of the random phase shifts leads to the additional decay constant γ_{phase}. This accounts for the largest effects of collisions. In practice γ (often referred to as $1/T_2$) can be considerably larger than γ_{ab}.

Equations (18) can be solved to any desired order in the perturbation $\mathcal{V}_{ab}(s,t)$. For incoherent pumping processes (those leaving ρ_{ab} unexcited) there are contributions to the diagonal components of ρ in even orders of $\mathcal{V}_{ab}$ and to the off-diagonal components in odd orders of $\mathcal{V}_{ab}$. The zeroth-order population difference is [from integration of (17) with $\mathcal{V}_{ab} = 0$]

$$N(s,v,t) = \rho_{aa}^{(0)}(s,v,t) - \rho_{bb}^{(0)}(s,v,t) = \frac{\lambda_a(s,v,t)}{\gamma_a} - \frac{\lambda_b(s,v,t)}{\gamma_b}. \tag{20}$$

We assume that the velocity distribution for the a and b levels is identical, and that the population difference can be factored as

$$N(s,v,t) = N(s,t)W(v).$$

Further, we assume that $N(s,t)$ has negligible variation in atomic lifetimes and the velocity distribution is Maxwellian,

$$W(v) = (u\pi^{1/2})^{-1} e^{-(v/u)^2},$$

where u is $2^{1/2}$ times the rms velocity.

Higher-order contributions to the matrix elements can be found from formal integrals of (18). In particular, one has for the off-diagonal (polarization) element

$$\rho_{ab}(s,v,t) = (i/\hbar)\int_{-\infty}^{t} dt'\, \mathcal{V}_{ab}(t')\exp[-(i\omega+\gamma)(t-t')][\rho_{aa}(s',v,t') - \rho_{bb}(s',v,t')]$$

$$= (i/\hbar)\int_{0}^{\infty} d\tau'\, \mathcal{V}_{ab}(t')\exp[-(i\omega+\gamma)\tau'][\rho_{aa}(s',v,t-\tau') - \rho_{bb}(s',v,t-\tau')], \tag{21}$$

where $\tau' = t - t'$, $s' = s - v\tau'$, and the perturbation interaction is integrated from $-\infty$ to the present. In evaluation of (21) and formulas to follow, it is helpful to remember that $t' = t - \tau'$. Similarly,

$$\rho_{aa}(s,v,t) - \rho_{bb}(s,v,t) = N(s,v,t) + \{(i/\hbar)\int_{0}^{\infty} d\tau'\,[\exp(-\gamma_a\tau') + \exp(-\gamma_b\tau')][\mathcal{V}_{ab}(t')\rho_{ba}(s',v,t-\tau') - \text{c.c.}]\}. \tag{22}$$

Saturation effects in the population difference arise from the bracketed expression in (22).

The $2n+1$ order of ρ_{ab} comes from evaluation of (21) using the $2n$ order of the population difference, which is similarly found from the bracketed portion of (22), using $\rho_{ab}^{(2n-1)}$. The total population matrix consists of summing the contributions from all orders considered in the calculation.

Using (20) in (21), we find the general first-order contribution to the off-diagonal element

$$\rho_{ab}^{(1)}(s,v,t) = iN(s,t)W(v)\hbar^{-1} \times \int_{0}^{\infty} d\tau'\exp[-(i\omega+\gamma)\tau']\mathcal{V}_{ab}(t'). \tag{23}$$

Substituting $\rho_{ab}^{(1)}$ into the appropriate portion of (22), we find the population-difference saturation term

$$\rho_{aa}^{(2)} - \rho_{bb}^{(2)} = -N(s,t)W(v)\hbar^{-2}\int_{0}^{\infty} d\tau' \times \int_{0}^{\infty} d\tau''[\exp(-\gamma_b\tau') + \exp(-\gamma_a\tau')]\mathcal{V}_{ab}(t') \times \exp[-(-i\omega+\gamma)'']\mathcal{V}_{ba}(t'') + \text{c.c.}, \tag{24}$$

where the interaction energy is possibly complex, $\mathcal{V}_{ba} = \mathcal{V}_{ab}^{*}$, and $\tau'' = t' - t''$. Finally, we find the third-order contribution to the off-diagonal element

$$\rho_{ab}^{(3)} = -iN(s,t)W(v)\hbar^{-3}\int_{0}^{\infty} d\tau'\int_{0}^{\infty} d\tau''\int_{0}^{\infty} d\tau'''\exp[-(i\omega+\gamma)\tau']\mathcal{V}_{ab}(t')[\exp(-\gamma_a\tau'') + \exp(-\gamma_b\tau'')] \times\{\mathcal{V}_{ba}(t'')\mathcal{V}_{ab}(t''')\exp[-(i\omega+\gamma)\tau'''] + \mathcal{V}_{ab}(t'')\mathcal{V}_{ba}(t''')\exp[-(-i\omega+\gamma)\tau'''\}], \tag{25}$$

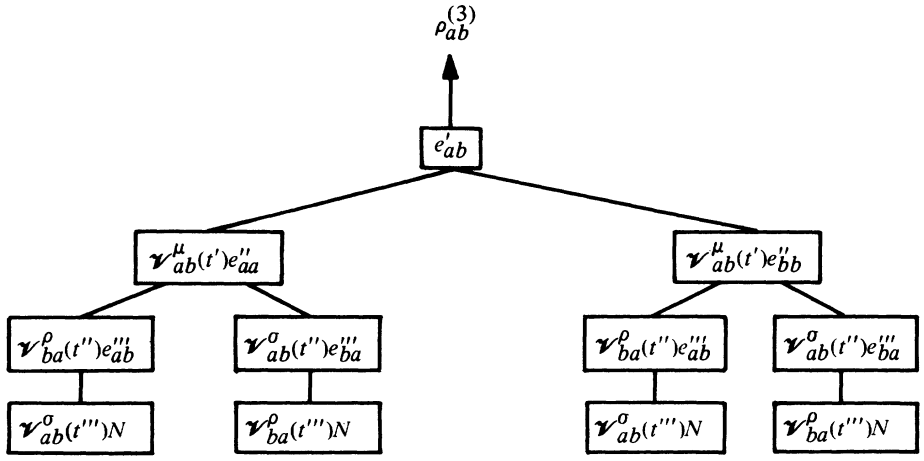

FIG. 3. Perturbation tree for calculation of the third-order matrix element $\rho_{ab}^{(3)}(s,v,t)$. The interaction energy $\mathcal{V}_{ab}$ is evaluated at earlier times and positions. The Greek superscript is the multimode summation index which we use for that level interaction. The symbols $e'_{\alpha\alpha} = (i/\hbar)\int_0^\infty d\tau' e^{-\gamma_\alpha\tau'}$, $e'_{\alpha\beta} = -e'_{\beta\alpha}{}^{*} = (i/\hbar)\int_0^\infty d\tau' e^{-(i\omega+\gamma)\tau'}$, and $N = \rho_{aa}^{(0)} - \rho_{bb}^{(0)} = N(s,v,t)$. The tree branches (products of four terms connected by descending lines) are labeled by t. The third-order contribution to $\rho_{ab}^{(3)}$ is given by the sum of the tree branches.

where $\tau''' = t'' - t'''$. It is also useful to remember that $t'' = t - \tau' - \tau''$ and $t''' = t - \tau' - \tau'' - \tau'''$ when particular $\mathcal{V}_{ab}$'s are substituted into (25).

It will be helpful to represent the third-order contribution (25) by a perturbation tree (Fig. 3) especially for the multimode-ring laser considered below. One finds $\rho_{ab}^{(3)}$ by multiplying terms connected by branch paths in the tree (vertically) and summing all the branch results (horizontally). The symbols $e_{\alpha\alpha}$ and $e_{\alpha\beta}$ stand for the time integral and exponential factor in the integrand of (22) and (21), e.g., $e_{\alpha\alpha} = (i/\hbar)\int d\tau \exp(-\gamma_\alpha \tau)$. Each branch point in Fig. 3 represents the sum in the integrand of the expressions for the population matrix elements. At the first branch level, the splitting is due to the ρ_{nn} and ρ_{bb} terms. The next branch level is split due to ρ_{ab} and ρ_{ba} contributions. The final branch has been consolidated, using (20) for $\rho_{aa}^{(0)} - \rho_{bb}^{(0)}$. The compact notation for the first ($t = 1$) branch in Fig. 3 is thus expanded to a portion of $\rho_{ab}^{(3)}$ in (25):

$$e'_{ab}\mathcal{V}_{ab}(t')e''_{aa}\mathcal{V}_{ba}(t'')e'''_{ab}\mathcal{V}_{ab}(t''')N - (i/\hbar)^3 \int_0^\infty d\tau' \exp[-(i\omega+\gamma)\tau']\mathcal{V}_{ab}(t')$$

$$\times \int_0^\infty d\tau'' \exp(-\gamma_a \tau'')\mathcal{V}_{ba}(t'') \int_0^\infty d\tau''' \exp[-(i\omega+\gamma)\tau''']\mathcal{V}_{ab}(t''')N(s, v, t). \tag{26}$$

The Greek superscript on $\mathcal{V}_{ab}$ in Fig. 3 is the multimode summation index which we use for that level interaction. The index ρ is always used for the complex conjugate ($\mathcal{V}_{ba}$) terms.

Using (2) for $E(s, t)$ and making the rotating-wave approximation in advance (i.e., neglecting negative-frequency components of $\mathcal{V}_{ab}$, since we know that they lead to terms which have large denominators compared to the positive-frequency terms), we find

$$\mathcal{V}_{ab}(s, t) = -\tfrac{1}{2}\wp \sum_n E_n(t)\exp[-i(\nu_n t + \phi_n)]U_n(s). \tag{27}$$

Evaluating the first order of ρ_{ab}, integrating over s and v, and projecting onto the nth mode, we obtain the first-order complex polarization

$$\mathcal{P}_n^{(1)} = -i\wp^2 E_n(\hbar\mathfrak{M})^{-1} \int_{-\infty}^\infty dv\, W(v) \int_0^L ds N(s, t)U_n^*(s)$$

$$\times \int_0^\infty d\tau' U_n(s - v\tau')\exp[-(i\omega - i\nu_n + \gamma)\tau']. \tag{28}$$

We have neglected terms oscillating at intermode frequencies in $\mathcal{P}_n^{(0)}$, because the high cavity Q restricts oscillation to frequencies close to the passive-cavity values. Aided by the perturbation tree (Fig. 3) for $\rho_{ab}^{(3)}$ we similarly evaluate the third-order contribution and find

$$\mathcal{P}_n^{(3)} = \frac{\mathfrak{M}^{-1}}{4} i\wp^4\hbar^{-3} \sum_\mu \sum_\rho \sum_\sigma E_\mu E_\rho E_\sigma \exp(i\psi_{n\mu\rho\sigma}) \int_0^L ds N(s, t)U_n^*(s)$$

$$\times \int_{-\infty}^\infty dv\, W(v) \int_0^\infty d\tau' \int_0^\infty d\tau'' \int_0^\infty d\tau''' \exp[-i(\omega - \nu_\mu + \nu_\rho - \nu_\sigma)\tau' - \gamma\tau']$$

$$\times\{\exp[-i(\nu_\rho - \nu_\sigma)\tau'' - \gamma_a\tau''] + \exp[-i(\nu_\rho - \nu_\sigma)\tau'' - \gamma_b\tau'']\}U_\mu(s - v\tau')$$

$$\times\{\exp[-i(\omega - \nu_\sigma)\tau''' - \gamma\tau''']U_\rho^*(s - v\tau' - v\tau'')U_\sigma(s - v\tau'' - v\tau'' - v\tau''')$$

$$+ \exp[-i(\nu_\rho - \omega)\tau''' - \gamma\tau''']U_\sigma(s - v\tau' - v\tau'')U_\rho^*(s - v\tau' - v\tau'' - v\tau''')\}, \tag{29}$$

where the relative phase angles are

$$\psi_{n\mu\rho\sigma} = (\nu_n - \nu_\mu + \nu_\rho - \nu_\sigma)t + (\phi_n - \phi_\mu + \phi_\rho - \phi_\sigma). \tag{30}$$

When we label the sums such that the subscript ρ remains with the complex conjugate ($\mathcal{V}_{ab}$) interaction term, all tree branches have the same relative phase angle.

In our discussion of laser mode intensities as functions of cavity tuning we will delineate the roles played by various mechanisms of population saturation. For this purpose we evaluate the population saturation term (24) for the multimode interaction energy (27),

$$\rho_{aa}^{(2)}-\rho_{bb}^{(2)}=-\tfrac{1}{4}(\wp/\hbar)^2N(s,t)W(v)\sum_\rho\sum_\sigma E_\rho E_\sigma\exp[i(\nu_\rho-\nu_\sigma)t+i(\phi_\rho-\phi_\sigma)]$$
$$\times\int_0^\infty d\tau'\int_0^\infty d\tau''\{\exp[-(i\nu_\rho-i\nu_\sigma+\gamma_a)\tau']+\exp[-(i\nu_\rho-i\nu_\sigma+\gamma_b)\tau']\}$$
$$\times\{\exp[-(i\nu_\rho-i\omega+\gamma)\tau'']U_\sigma(s-v\tau')U_\rho(s-v\tau'-v\tau'')$$
$$+\exp[-(i\omega-i\nu_\sigma+\gamma)\tau'']U_\rho(s-v\tau')U_\sigma(s-v\tau'-v\tau'')\}. \tag{31}$$

We see that most of the saturation terms vary in time at intermode frequencies. These lead to the "population pulsations." Whenever $\rho=\sigma$, the population saturation is time invariant. These constant terms are generally larger than the oscillating terms by about $(\nu_\rho-\nu_\sigma)/\gamma_a$ and give rise to hole burning. We now investigate particular solutions for the complex polarization $\mathcal{P}_n\approx\mathcal{P}_n^{(1)}+\mathcal{P}_n^{(3)}$, choosing different mode sets $U_n(s)$.

IV. UNIDIRECTIONAL-RING AND STANDING-WAVE LASERS

The simplest case to evaluate, but nevertheless one of practical importance, is the unidirectional-ring laser. This laser has been made to operate by use of a Faraday rotator in conjunction with Brewster angle surfaces inside the cavity,[16] thus preferentially reducing the cavity Q for radiation propagating in one direction. The modes are traveling waves moving in only one direction; i.e., K_n is positive. Substituting (3) into (28), we find the first-order complex polarization

$$\mathcal{P}_n^{(1)}=\wp^2(Ku\hbar)^{-1}E_n\bar{N}Z[\gamma+i(\omega-\nu_n)], \tag{32}$$

where the excitation density is

$$\bar{N}=(1/L)\int_0^L dsN(s,t) \tag{33}$$

and the plasma dispersion function is

$$Z(v)=iK\pi^{-1/2}\int_0^\infty d\tau'\int_{-\infty}^\infty dv\exp[-(v/u)^2]$$
$$\times\exp[-(v+iKv)\tau']$$
$$=cK\pi^{-1/2}\int_{-\infty}^\infty dv\exp[-(v/u)^2]/(v+iKv). \tag{34}$$

Other equivalent definitions and some properties of the plasma dispersion function are found in the Appendix. Similarly, substituting (3) into (29) we find the third-order complex polarization

$$\mathcal{P}_n^{(3)}(t)=\tfrac{1}{4}(i\wp^4/\hbar^3)\sum_\mu\sum_\rho\sum_\sigma E_\mu E_\rho E_\sigma\exp(i\psi_{n\mu\rho\sigma})\left(\frac{1}{L}\right)\int_0^L dsN(s,t)\exp(-iK_ns)\int_{-\infty}^\infty dv\,W(v)$$
$$\times\int_0^\infty d\tau'\int_0^\infty d\tau''\int_0^\infty d\tau'''\exp\{-[i(\omega-\nu_\mu+\nu_\rho-\nu_\sigma)+\gamma]\tau'\}$$
$$\times(\exp\{-[i(\nu_\rho-\nu_\sigma)+\gamma_a]\tau''\}+\exp\{-[i(\nu_\rho-\nu_\sigma)+\gamma_b]\tau''\})\exp[iK_\mu(s-v\tau')] \tag{35}$$
$$\times[\exp\{-[i(\omega-\nu_\sigma)+\gamma]\tau'''\}\exp\{-iK_\rho[s-v(\tau'+\tau'')]\}\exp\{+iK_\sigma[s-v(\tau'+\tau''+\tau''')]\}$$
$$+\exp\{-[i(\nu_\rho-\omega)+\gamma]\tau'''\}\exp\{-iK_\rho[s-v(\tau'+\tau''+\tau''')]\}\exp\{+iK_\sigma[s-v(\tau'+\tau'')]\}),$$

where the relative phase angles $\psi_{n\mu\rho\sigma}$ are given by (30).

As in the first-order polarization (Eq. 28), we neglect terms which oscillate at intermode beat frequencies. Here this results in retaining only terms satisfying the relation

$$n=\mu-\rho+\sigma. \tag{36}$$

With this constraint, the wave number K_n equals $n\pi/L=(\mu-\rho+\sigma)\pi/L$, and the integral over the laser path length reduces to the average excitation density $\bar{N}$ for all terms in the summations. Further, since $Ku\ll\nu$, we let $K_\mu v=K_\rho v=K_\sigma v=Kv$ in the time integrals. With these considerations (35) becomes

$$\mathcal{P}_n^{(3)}(t)=\tfrac{1}{4}\wp^4\frac{\bar{N}}{\hbar^3Ku}\sum_\mu\sum_\rho\sum_\sigma E_\mu E_\rho E_\sigma\exp[i\psi_{n\mu\rho\sigma}]\int_\infty^\infty dv\exp[-(v/u)^2]\int_0^\infty d\tau'\int_0^\infty d\tau''\int_0^\infty d\tau'''\exp(-v_{11}\tau')$$
$$\times[\exp(-v_{12}\tau'')+\exp(-v_{42}\tau'')]\{\exp[-v_{13}\tau'''-iKv(\tau'+\tau''')]+\exp[-v_{43}\tau'''-iKv(\tau'-\tau''')]\}, \tag{37}$$

where the complex frequencies v_{tk} are defined in Table I, and the Maxwellian distribution has been used for $W(v)$. The subscript t refers to the branch number of Fig. 3. The integrals in (37) are particular examples of the standard form

$$T = iK\pi^{-1/2}\int_{-\infty}^{\infty} dv\,\exp[-(v/u)^2]\int_0^{\infty} d\tau'\int_0^{\infty} d\tau''\int_0^{\infty} d\tau'''\,\exp[-(v_1+ic_1Kv)\tau' - (v_2+ic_2Kv)\tau'' - (v_3+ic_3Kv)\tau''']$$

$$= iK\pi^{-1/2}\int_{-\infty}^{\infty} dv\,\exp[-(v/u)^2]/[(v_1+ic_1Kv)(v_2+ic_2Kv)(v_3+ic_3Kv)]\,. \tag{38}$$

This integral can be expressed in terms of the plasma dispersion function (34) by the method of partial fractions, as shown in the Appendix. The value of T depends markedly on the constants c_1, c_2, and c_3. Only certain combinations of c's appear in the laser theory. We find it convenient to distinguish between the T's occurring in the present theory by assigning a subscript w as defined in Table II. In the unidirectional calculation only $w = 1$ and 2 time dependences are found. Further affixing the branch index t of Fig. 3, we write the integral (38)

$$T_{tw} = iK\pi^{-1/2}\int_{-\infty}^{\infty} dv\,\exp[-(v/u)] \times[(v_{t1}+ic_{w1}Kv)(v_{t2}+ic_{w2}Kv)(v_{t3}+ic_{w3}Kv)]^{-1}\,, \tag{39}$$

in which v_{tk} and the c_{wk} are defined in Tables I and II, respectively. In this notation, the third-order polarization (37) is

$$\mathcal{P}_n^{(3)} = \tfrac{1}{4}\left(\frac{\overline{N}\wp^4}{\hbar^3 Ku}\right)\sum_{\mu}\sum_{\rho}\sum_{\sigma} E_\mu E_\rho E_\sigma \times e^{i\psi_{n\mu\rho\sigma}}(T_{12}+T_{21}+T_{31}+T_{42})\,. \tag{40}$$

As an example, we examine a laser whose Doppler width Ku is much larger than the atomic decay rates $\gamma, \gamma_a, \gamma_b$, as well as various frequency differences $\omega - \nu_n$, etc. This is the "strong Doppler limit" of the Appendix for which the T_{tw} reduce to

$$T_{t1} \simeq 2i\pi^{1/2}[v_{t2}(v_{t1}+v_{t3})]^{-1}\,,\quad T_{t2}\simeq T_{t3}\simeq 0\,. \tag{41}$$

The third-order complex polarization then becomes

$$\mathcal{P}_n^{(3)} = \tfrac{1}{4}i\pi^{1/2}\wp^4\overline{N}(\hbar^3 Ku)^{-1}\sum_{\mu}\sum_{\rho}\sum_{\sigma} E_\mu E_\rho E_\sigma e^{i\psi_{n\mu\rho\sigma}} \times[\mathfrak{D}_a(\nu_\rho-\nu_\sigma)+\mathfrak{D}_b(\nu_\rho-\nu_\sigma)]\mathfrak{D}(\nu_\rho-\tfrac{1}{2}\nu_\mu-\tfrac{1}{2}\nu_\sigma)\,, \tag{42}$$

where $\mathfrak{D}(\Delta\omega)$ stands for the frequently recurring denominator

$$\mathfrak{D}_x(\Delta\omega) = 1/(\gamma_x + i\Delta\omega)\,. \tag{43}$$

Numerical results and physical discussions are given in Secs. V – VII.

Using a similar analysis, we investigate the two-mirror standing-wave laser. For this case, the boundary conditions require that the electric field be superpositions of standing waves throughout the cavity. The modes selected are given by (4), where L is now the one-way cavity length. Since the velocity distribution is assumed to be even, only the even portions of the expansions of sines give nonzero contributions to the velocity integrals. Thus

$$\sin K_n(s - v\tau') \to \sin K_n s\cos K_n v\tau'$$

only for this calculation.

Substituting (4) into (22), we find the first-order complex polarization

$$\mathcal{P}_n^{(1)}(t) = \wp^2[\hbar Ku]^{-1}\overline{N}E_n(t)Z[\gamma + i(\omega - \nu_n)]\,, \tag{44}$$

which is the same result as that (32) for the unidirectional ring. We have neglected a contribution containing the integral

$$\int_0^L N(st)\cos(2K_n s)\,ds\,,$$

which averages to zero since $N(s,t)$ varies little in an optical wavelength.

TABLE I. Definitions of complex frequencies v_{tk} appearing in the third-order integrals (39).

v_{tk}	$k=1$	$k=2$	$k=3$
$t=1$	$\gamma+i(\omega-\nu_\mu+\nu_\rho-\nu_\sigma)$	$\gamma_a+i(\nu_\rho-\nu_\sigma)$	$\gamma+i(\omega-\nu_\sigma)$
2	$\gamma+i(\omega-\nu_\mu+\nu_\rho-\nu_\sigma)$	$\gamma_a+i(\nu_\rho-\nu_\sigma)$	$\gamma+i(\nu_\rho-\omega)$
3	$\gamma+i(\omega-\nu_\mu+\nu_\rho-\nu_\sigma)$	$\gamma_b+i(\nu_\rho-\nu_\sigma)$	$\gamma+i(\nu_\rho-\omega)$
4	$\gamma+i(\omega-\nu_\mu+\nu_\rho-\nu_\sigma)$	$\gamma_b+i(\nu_\rho-\nu_\sigma)$	$\gamma+i(\omega-\nu_\sigma)$

TABLE II. Definitions of the constants c_{wk} used in the third-order integrals (39). The total time dependence in (39) is given by x_w.

c_{wk}	$k=1$	2	3	$x_w = c_{w1}\tau' + c_{w2}\tau'' + c_{w3}\tau'''$
$w=1$	1	0	−1	$\tau' - \tau'''$
2	1	0	1	$\tau' + \tau'''$
3	1	2	1	$\tau' + 2\tau'' + \tau'''$

The third-order contribution to the polarization (29) involves two products of four sine functions, each sine evaluated at a different initial point in time. One of these products can be expanded to

$$\tfrac{1}{8}\{\cos[(K_n - K_\mu - K_\rho + K_\sigma)s]\cos[Kv(\tau''' - \tau')] + \cos[(K_n - K_\mu + K_\rho - K_\sigma)s]\cos[Kv(\tau''' + \tau')] + \cos[K_n + K_\mu - K_\rho - K_\sigma)s]\cos[Kv(\tau''' + 2\tau'' + \tau')]\}, \tag{45}$$

while the other is given by (45) with the indices ρ and σ interchanged. We have again retained only the slowly varying part, which is even in v.

In the unidirectional calculation, the space and time dependence of the mode functions separated trivially, and the spatial portion became constant when the slowly varying restraint (36) was imposed. In the present case, as well as the bidirectional ring (Sec. V), the space and time dependence still separates, but the spatial dependence is more complicated. However, the separability of the product of four-mode functions allows us to examine the integral over the excitation density separately. In general, this integral depends on the mode indices n, μ, ρ, and σ, and can be written

$$N_{n\mu\rho\sigma} = \mathfrak{M}^{-1}\int_0^L ds N(s,t) f_{n\mu\rho\sigma}(s), \tag{46}$$

including the normalization factor $\mathfrak{M}$; $f_{n\mu\rho\sigma}(s)$ is some function of position s alone. For the standing-wave laser, there are three possible values of $f_{n\mu\rho\sigma}(s)$ which are given in (45). With the constraint $n = \mu - \rho + \sigma$, the excitation integrals take the form

TABLE III. Definitions of the excitation integral N_{tw} in terms of N_{2l} (47) for the standing-wave laser and N_2 (53) for the traveling-wave laser.

N_{tw}	$w=1$	2	3
$t=1$	$N_2(\rho-\sigma)$	$\bar{N}$	$N_2(\rho-\mu)$
2	$\bar{N}$	$N_2(\rho-\sigma)$	$N_2(\rho-\mu)$
3	$\bar{N}$	$N_2(\rho-\sigma)$	$N_2(\rho-\mu)$
4	$N_2(\rho-\sigma)$	$\bar{N}$	$N_2(\rho-\mu)$

$$N_{n\mu\rho\sigma} = 2N_{2l} = (2/L)\int_0^L ds N(s,t)\cos(2l\pi s/L) \tag{47}$$

for any of the functions of s in (46). We call the small-integer difference of two-mode indices l.

Substituting (45) in (29) and writing the time-dependent consine functions as exponentials, we again find the third-order integrals of the form (39). Note that the sign of Kv is immaterial in (39). The indices t and w are still associated with the perturbation tree branch and time dependence, respectively. The v_{tk} and c_{wk} are found in Tables I and II. With these conventions, $\mathcal{P}_n^{(3)}$ is written

$$\mathcal{P}_n^{(3)} = \left(\frac{\wp^4}{(16\hbar^3 Ku)}\right)\sum_\mu\sum_\rho\sum_\sigma E_\mu E_\rho E_\sigma \times e^{i\psi_{n\mu\rho\sigma}}\sum_{t=1}^{4}\sum_{w=1}^{3} T_{tw}N_{tw}, \tag{48}$$

with N_{tw} given in terms of N_{2l} in Table III and T_{tw} given by (37). In the strong Doppler limit of (41) this expression reduces to

$$\mathcal{P}_n^{(3)}(t) = \tfrac{1}{16}i\pi^{1/2}\wp^4(\hbar^3 Ku)^{-1}\sum_\mu\sum_\rho\sum_\sigma E_\mu E_\rho E_\sigma \exp(i\psi_{n\mu\rho\sigma})[\mathfrak{D}_a(\nu_\rho - \nu_\sigma) + \mathfrak{D}_b(\nu_\rho - \nu_\sigma)] \times [N_{2(\rho-\sigma)}\mathfrak{D}(\omega - \tfrac{1}{2}\nu_\mu + \tfrac{1}{2}\nu_\rho - \nu_\sigma) + \bar{N}\mathfrak{D}(-\tfrac{1}{2}\nu_\mu - \tfrac{1}{2}\nu_\sigma + \nu_\rho)]. \tag{49}$$

V. BIDIRECTIONAL-RING LASER

Many experimenters have investigated the bidirectional-ring laser, encouraged by its use as a rotation rate sensor. Several researchers have applied theories based on Lamb's model to the ring laser. Aronowitz[4] originally developed this theory for a two-mode laser with one traveling-wave mode in each direction. Note that while "mode" refers to a standing wave in a two-mirror laser, it denotes a traveling wave in a ring laser since both sine *and* cosine can exist. Close[17] investigated the population excitation density for two traveling waves in the same direction. Whitney[18] obtained mode-coupling relations in the limit of no population pulsations. As mentioned above, the two-mode ring laser has been investigated using a theory applicable to high intensity by Mennegozzi and Lamb.[4] Miyashita, Mori, and Ikenoue[19] have applied Lamb's theory to investigate phase locking in special cases of ring-laser operation.

We chose the electric field for the ring laser to be a sum of waves traveling in both the positive and negative s directions. The field is periodic but not necessarily a superposition of standing waves. While the two-mirror standing-wave laser field is also composed of positive and negative traveling waves, the amplitudes, frequencies, and phases of oppositely directed waves with the same K_n have the same values. These degeneracies

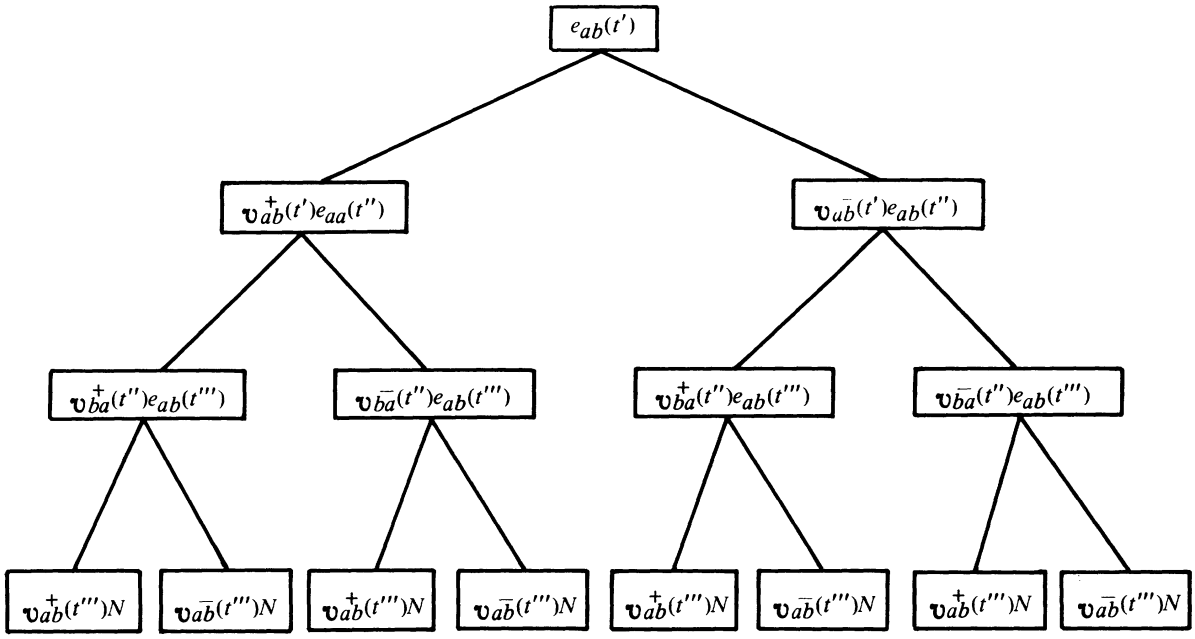

FIG. 4. First branch ($t = l$) of the expanded perturbation tree for the general ring laser. $\mathcal{V}_{ab} = \mathcal{V}^{+}_{ab} + \mathcal{V}^{-}_{ab}$, where the sign superscript refers to the direction of the traveling-wave modes. Other notation is the same as in Fig. 3.

are removed in the ring laser. It is convenient to index the traveling-wave modes by the subscript n. Thus the interaction energy matrix element is

$$\mathcal{V}_{ab}(s,t) = -\tfrac{1}{2}\wp \sum_n E_n(t) \exp\{-i[\nu_n t + \phi_n(t) - K_n s]\}, \tag{50}$$

where $K_n = 2n\pi/L$ and n is negative for waves running in the $-s$ direction. Here L is the round-trip cavity length for the stationary cavity. In general, the phase factor may depend on both s and t. However for uniformity with previous cases, we neglect the s dependence.

From (28) we find that the first-order contribution to the nth polarization component is given by

$$\mathcal{P}^{(1)}_n(t) = -\wp^2 \overline{N}[\hbar K u]^{-1} E_n(t) Z[\gamma + i(\omega - \nu_n)]. \tag{51}$$

It is now useful to expand the perturbation tree in Fig. 3, decomposing $\mathcal{V}_{ab}$ into the sum of its positive $\mathcal{V}^{+}$, negative $\mathcal{V}^{-}$ running waves, that is, $\mathcal{V}_{ab} = \mathcal{V}^{+}_{ab} + \mathcal{V}^{-}_{ab}$. The first branch ($t = 1$) of such an expanded tree is shown in Fig. 4. The third-order contribution ρ_{ab} is found by summing the products of the integrals operating vertically. In the expanded tree, there are 32 separate third-order time integrals arising from the direction of travel of the modes. Each level of the tree in Fig. 3 is doubled, producing 2^3 times as many terms in $\rho^{(3)}_{ab}$. Fortunately, it is not necessary to explicitly write the sum from the perturbation tree for $\rho^{(3)}_{ab}$. Rather, we can find $\rho^{(3)}_{ab}$ from a table (Table IV) which contains only the distinguishing characteristics of the tree branches.

From (50) we see that the time and space parts of the $U_\mu(s)$, etc., separate easily. The dependence on the present time t leads to the usual relative phase angle $\psi_{n\mu\rho\sigma}$ in $\mathcal{P}^{(3)}_n$, while the spatial dependence goes into the general excitation integral. Since $\psi_{n\mu\rho\sigma}$ does not explicitly depend on the mode directions, the restriction to slowly varying relative phases again requires $|n| = |\mu| - |\rho| + |\sigma|$. The excitation integral can then be written

TABLE IV. Definitions of the excitation integral (53) as a function of traveling-wave directions of the interacting modes. A given set of directions only contributes to the complex polarization of modes traveling in one direction. These integrals are related to the N_{tw} format in Table IV. Two combinations always lead to rapidly varying integrands in (53).

$\mathrm{sgn}(K_\mu)$	$\mathrm{sgn}(K_\rho)$	$\mathrm{sgn}(K_\sigma)$	$\mathrm{sgn}(K_n)$	$\mathfrak{N}_{2l}$
+	+	+	+	$\mathfrak{N}_0 = \overline{N}$
+	+	−	−	$\mathfrak{N}_2(\rho - \mu)$
+	−	+		none
+	−	−	+	$\mathfrak{N}_2(\rho - \sigma)$
−	+	+	−	$\mathfrak{N}_2(\rho - \sigma)$
−	+	−		none
−	−	+	+	$\mathfrak{N}_2(\rho - \mu)$
−	−	−	−	$\mathfrak{N}_0 = \overline{N}$

$$N_{n\mu\rho\sigma} = (1/L)\int_0^L ds N(s,t)\exp[-i(K_n - K_\mu + K_\rho - K_\sigma)s], \tag{52}$$

including the normalization factor $\mathfrak{M} = L^{-1}$ and the slowly varying phase restriction. Since $N(s,t)$ varies slowly, the non-negligible contributions to $N_{n\mu\rho\sigma}$ occur only when the exponential term is slowly varying also. Thus only certain combinations of positive and negative running waves are allowed. All of the non-negligible excitation integrals can be written in the form

$$\mathfrak{N}_{2l} = (1/L)\int_0^L ds N(s,t)e^{-i4\pi ls/L}, \tag{53}$$

where l is a small integer $0, \pm1, \pm2, \ldots$. Table IV gives the permissible combinations, as well as relating these to the N_{tw} format of Table III. Note that the complex excitation integrals are related to the real integrals (47) of the standing-wave case by

$$\mathfrak{N}_{2|l|} + \mathfrak{N}_{-2|l|} \xrightarrow[L\to 2L]{} 2N_{2|l|}.$$

The third-order complex polarization is given by

$$\mathcal{P}_n^{(3)} = \tfrac{1}{4}\wp^4(\hbar^3 Ku)\sum_\mu\sum_\rho\sum_\sigma E_\mu E_\rho E_\sigma e^{i\psi_{n\mu\rho\sigma}}\sum_{t=1}^{4} N_{tw}T_{tw}, \tag{54}$$

where T_{tw} is defined by (39) and N_{tw} by Table IV. Here the sums over the mode directions determine w instead of the explicit sum appearing in the standing-wave case [Eq. (48)]. The value of w is given by the combination of running waves as defined in Table V, where the sum over the traveling-wave directions is explicitly recorded (or equivalently, the perturbation tree branches are summed).

Note that if we let $\mathfrak{V}^- = 0$, the general ring results collapse to the unidirectional results of Sec. IV. Alternatively, if we assume

$$\begin{aligned} &E_{n+}(t) = E_{n-}(t) = \tfrac{1}{2}E_n(t),\\ &\nu_{n+} = \nu_{n-} = \nu_n,\\ &\phi_{n+}(t) = \phi_n(t) + \tfrac{1}{2}\pi,\\ &\phi_{n-}(t) = \phi_n(t) - \tfrac{1}{2}\pi,\\ &L_{\text{ring}} \to 2L_{\text{standing wave}}, \end{aligned} \tag{55}$$

the general ring reduces to the standing-wave laser, as it should.

TABLE V. Summary of the calculation of the T_{tw} for $\mathcal{P}_n^{(3)}(t)$ of the general ring laser. The direction of travel of the interacting modes are given by the d_n's[$=\mathrm{sgn}(K_n)$]. The variables s', s'' and s''' give the signs (±1) of the coefficients of $-Kv\tau'$, $-Kv(\tau'+\tau'')$ and $-Kv(\tau'+\tau''+\tau''')$ in (29), respectively. For the μ terms, s' is always associated with K_μ and hence has the same sign. The ρ terms are correlated so that s'' and s''' has the opposite sign from d_ρ when associated with ρ (see column under t for associations). Hence for $t=1$ (depicted in Fig. 4), $\mathfrak{V}_{ba}$ occurs for $\tau'+\tau''$ and s'' has the opposite sign from K_ρ. When s'' and s''' are associated with K_σ they have the same sign as K_σ. The sum $s'\tau' + s''(\tau'+\tau'') + s'''(\tau'+\tau''+\tau''')$ is given by

$$(s'+s''+s''')\tau' + (s''+s''')\tau'' + s'''\tau''' = c_1\tau' + c_2\tau'' + c_3\tau'''$$

which yields the c's in Table II defining the subscript w of T_{tw}. Table V is worth understanding because it takes the place of a tremendous amount of algebra.

t	d_μ	d_ρ	d_σ	s'	s''	s'''	w	T_{tw}
	+	+	+	+1	−1	+1	2	T_{t2}
1 or 4	+	+	−	+1	−1	−1	3	T_{t3}
	+	−	+	+1	+1	+1	none[a]	0
$\mu \leftrightarrow \tau'$	+	−	−	+1	+1	−1	1	T_{t1}
$\rho \leftrightarrow \tau''$	−	+	+	−1	−1	+1	1	T_{t1}
$\sigma \leftrightarrow \tau'''$	−	+	−	−1	−1	−1	none[a]	0
	−	−	+	−1	+1	+1	3	T_{t3}
	−	−	−	−1	+1	−1	2	T_{t2}
	+	+	+	+1	+1	−1	1	T_{t1}
2 or 3	+	+	−	+1	−1	−1	3	T_{t3}
	+	−	+	+1	+1	+1	none[a]	0
$\mu \leftrightarrow \tau'$	+	−	−	+1	−1	+1	2	T_{t2}
$\rho \leftrightarrow \tau'''$	−	+	+	−1	+1	−1	2	T_{t2}
$\sigma \leftrightarrow \tau''$	−	+	−	−1	−1	−1	none[a]	0
	−	−	+	−1	+1	+1	3	T_{t3}
	−	−	−	−1	−1	+1	1	T_{t1}

[a] These terms contain rapidly varying integrands in z and hence vanish.

In the strong Doppler limit of (52), we note that only two sets of mode direction combinations lead to non-negligible terms. These are (i) all modes in the same direction and (ii) modes n, μ, and σ in one direction and ρ in the other. For the time being we specifically indicate the direction of travel of a mode by adding a subscript + or −. With these conventions, the complex polarization of the positive traveling mode of wave number K_{n+} is

$$\begin{aligned}\mathcal{P}_{n+}^{(3)} = i\pi^{1/2}\wp^4(4\hbar^3 Ku)^{-1}\sum_\mu\sum_\rho\sum_\sigma\{&E_{\mu+}E_{\rho+}E_{\sigma+}[\mathfrak{D}_a(\nu_{\rho+}-\nu_{\sigma+}) + \mathfrak{D}_b(\nu_{\rho+}-\nu_{\sigma+})]\\ &\times\overline{N}\mathfrak{D}(-\tfrac{1}{2}\nu_{\mu+} + \nu_{\rho+} + -\tfrac{1}{2}\nu_{\sigma-})e^{i\psi_{n+,\mu+,\rho+,\sigma+}} + E_{\mu+}E_{\rho-}E_{\sigma-}\\ &\times[\mathfrak{D}_a(\nu_{\rho-}-\nu_{\sigma-}) + \mathfrak{D}_b(\nu_{\rho-}-\nu_{\sigma-})]_{2(\rho-\sigma)}\mathfrak{D}(\omega - \tfrac{1}{2}\nu_{\mu+} + \tfrac{1}{2}\nu_{\rho-} - \nu_{\sigma-})\, e^{i\psi_{n+,\mu+,\rho-,\sigma-}}\}. \end{aligned} \tag{56}$$

Here, for example, the relative phase angle is

$$\psi_{n+,\mu+,\rho-,\sigma-} = (\nu_{n+} - \nu_{\mu+} + \nu_{\rho-} - \nu_{\sigma-})t + (\phi_{n+} - \phi_{\mu+} + \phi_{\rho-} - \phi_{\sigma-}) .$$

The negative traveling-mode result is obtained by changing all + and – signs.

VI. GENERAL FIELD EQUATIONS AND FREE-RUN APPROXIMATION

When the expressions for the complex polarization $\mathcal{P}_n^{(t)} \approx \mathcal{P}_n^{(1)} + \mathcal{P}_n^{(3)}$, derived in terms of the field amplitudes E_n in previous sections, are substituted in the self-consistency equations (8), we find a set of coupled differential equations which determine the amplitudes and frequencies of the laser modes. For the general case describing the unidirectional- and bidirectional-ring lasers, as well as the two-mirror (standing-wave) laser, the equations are written

$$\dot{E}_n = \alpha_n E_n - \sum_{\mu}\sum_{\rho}\sum_{\sigma} E_\mu E_\rho E_\sigma \times \mathrm{Im}(\vartheta_{n\mu\rho\sigma} e^{i\psi_{n\mu\rho\sigma}}) , \tag{57}$$

$$\nu_n + \dot{\phi}_n = \Omega_n + \sigma_n - \sum_{\mu}\sum_{\rho}\sum_{\sigma} E_\mu E_\rho E_\sigma E_n^{-1} \times \mathrm{Re}(\vartheta_{n\mu\rho\sigma} e^{i\psi_{n\mu\rho\sigma}}) ,$$

where the coefficients are summarized in Tables VI and VII.

In these equations E_n, ν_n, Ω_n, and ϕ_n are the electric field amplitudes, oscillation frequencies, passive-cavity frequencies, and phases, respectively, defined in Eqs. (2) and (8). The relative phase angles $\psi_{n\mu\rho\sigma}$ are defined by (30). In the remainder of this section we discuss the multimode "free-run" case of the amplitude- and frequency-determining equations in general terms. In Sec. VII two-mode cases are used to illustrate the formalism and physical processes. Finally, in Sec. VIII numercial cases of multimode operation are given.

We will find it useful to express the coefficients in (57) in terms of the relative excitation

$$\mathfrak{N} = \bar{N}/\bar{N}_{\text{threshold}} = \bar{N}\wp^2 Q Z_i(\gamma)(\hbar K u \epsilon_0)^{-1} , \tag{58}$$

in which the threshold excitation $N_{\text{threshold}}$ is determined by setting the linear net gain coefficient α_n to zero at line center. In Table VI, the use of the relative excitation is included as an alternate definition of the first-order factor F_1. Together with the notation for dimensionless intensities (61) introduced below, this representation establishes a uniform notation independent of the electric-dipole matrix element $\wp$, which is often not known directly.

We have already invoked the constraint that the relative phase angles be slowly varying, i.e., $n = \mu - \rho + \sigma$. There are three groups of mode indices which satisfy this requirement:

TABLE VI. Summary of coefficients appearing in the amplitude and frequency determining Eq. (57). The primes are dropped for two-mirror and unidirectional ring configurations. Variables used here are defined by equations as follows: Z_r and Z_i are the real and imaginary parts of the plasma dispersion function $Z(\nu)^i$ of Eq. (34), γ is the polarization decay constant ($1/T_2$ in NMR language) of Eq. (19), ω is the atomic resonance frequency (Fig. 2), ν_n is the frequency of the nth mode, Q_n is the quality factor of the nth mode, N_{tw} is the excitation component defined in Table III, T_{tw} is the third-order velocity integral (39) with frequencies and constants given in Tables I and II.

Coefficient	Physical context
$\alpha_n = Z_i[\gamma + i(\omega - \nu_n)]F_1 - \nu/2Q_n$	Linear net gain (all configurations)
$\sigma_n = Z_r[\gamma + i(\omega - \nu_n)][(\omega - \nu_n)/\gamma]F_1$	Linear mode pulling (all configurations)
$\vartheta_{n\mu\rho\sigma} = F_3 \sum_{t=1}^{4} (N_{tw}/\bar{N}) T_{tw}$	Complex saturation coefficient (bidirectional ring)
$\vartheta_{n\mu\rho\sigma} = F_3 \sum_{t=1}^{4}\sum_{w=1}^{3} (N_{tw}/\bar{N}) T_{tw}$	Complex saturation coefficient (two-mirror laser)
$\vartheta_{n\mu\rho\sigma} = (T_{12} + T_{21} + T_{31} + T_{42})F_3$	Complex saturation coefficient (unidirectional ring)
$F_1 = \frac{1}{2}\nu\wp^2 N(\hbar K u \epsilon_0)^{-1}$	First-order factor
$= \nu\mathfrak{N}[2QZ_i(\gamma)]^{-1}$	First-order factor with relative excitation $\mathfrak{N}$ of (59)
$F_3 = (\wp/2\hbar)^2 F_1$	Third-order factor

(a) $n=\mu,\ \rho=\sigma=m$,

(b) $n=\sigma,\ \mu=\rho=m$, (59)

(c) $n+\rho=\mu+\sigma$ [excluding (a) and (b)].

The first group results from hole burning, that is, reduced population inversion due to transitions induced by the fields. The second group results from population pulsations discussed in connection with the second-order population difference expression (31). The third group (also resulting from population pulsations) gives rise to the combination tone terms, which act as injected signals to induce phase locking. At present we seek steady-state solutions for free-running lasers and assume that effects coming from the combination tones average out, and that there is no phase (mode) locking. We retain in the calculation only terms in groups (a) and (b), which are phase independent. This constitutes the *free-run approximation* for which the amplitude and frequency equations are explicitly decoupled, since only terms with $\psi_{n\mu\rho\sigma}\equiv 0$ are retained. The equations of motion for the dimensionless mode intensities become

$$I_n=\tfrac{1}{2}(\wp E_n/\hbar)^2(\gamma_a\gamma_b)^{-1}, \tag{60}$$

$$\dot{I}_n=2I_n\left(\alpha_n-\sum_m\theta_{nm}I_m\right). \tag{61}$$

The saturation coefficients are now expressed as

$$\theta_{nm}=2\gamma_a\gamma_b\hbar^2\wp^{-2}\,\mathrm{Im}\{\vartheta_{nnmm}+\vartheta_{nmmn}\}(1-\tfrac{1}{2}\delta_{nm}), \tag{62}$$

where δ_{nm} is the Kronecker δ.

TABLE VII. Formulas for the general saturation coefficient $\vartheta_{n\mu\rho\sigma}$ of Table VI and Eqs. (57) for the unidirectional-ring, two-mirror, and bidirectional-ring lasers in both Doppler and homogeneously broadened limits. With use of (55), reduction of the bidirectional ring case to the two-mirror case is easily seen in all cases.

$\vartheta_{n\mu\rho\sigma}$	Approximation
Unidirectional-ring laser	
$\vartheta^{\text{uni-Dop}}\equiv\mathfrak{F}(\nu_\rho-\nu_\sigma)\mathfrak{D}(-\frac{1}{2}\nu_\mu-\frac{1}{2}\nu_\sigma+\nu_\rho)$	Doppler limit
$\vartheta^{\text{uni-ho}}\equiv\mathfrak{F}(\nu_\rho-\nu_\sigma)\mathfrak{D}(\omega-\nu_\mu+\nu_\rho-\nu_\sigma)\times[\mathfrak{D}(\omega-\nu_\sigma)+\mathfrak{D}(\nu_\rho-\omega)]$	Homogeneously broadened limit
Two-mirror Standing-wave laser	
$\frac{1}{4}\mathfrak{F}(\nu_\rho-\nu_\sigma)[\mathfrak{D}(\omega-\frac{1}{2}\nu_\mu-\frac{1}{2}\nu_\rho-\nu_\sigma)N_{2(\rho-\sigma)}\sqrt{\bar{N}}+\mathfrak{D}(-\frac{1}{2}\nu_\mu-\frac{1}{2}\nu_\sigma+\nu_\rho)]$	Doppler limit
$\frac{1}{4}\mathfrak{F}(\nu_\rho-\nu_\sigma)[1+(N_{2(\rho-\sigma)}+N_{2(\rho-\mu)})/\bar{N}]\times\mathfrak{D}(\omega-\nu_\mu+\nu_\rho-\nu_\sigma)[\mathfrak{D}(\omega-\nu_\sigma)+\mathfrak{D}(\nu_\rho-\omega)]$	Homogeneously broadened limit
$\mathfrak{F}(\nu_\rho-\nu_\sigma)=i(\frac{1}{2}\wp/\hbar)^2[\mathfrak{D}_a(\nu_\rho-\nu_\sigma)+\mathfrak{D}_b(\nu_\rho-\nu_\sigma)]$	
Bidirectional-ring laser	
d_n d_μ d_ρ d_σ ($d_n=\mathrm{sgn}(K_n)$, etc.)	
$+\ +\ +\ +$ / $-\ -\ -\ -$: $\vartheta^{\text{uni-Dop}}$	Doppler limit
$+\ +\ -\ -$ / $-\ -\ +\ +$: $\mathfrak{F}(\nu_\rho-\nu_\sigma)[\mathfrak{N}_{2(\rho-\sigma)}\sqrt{\bar{N}}]\times\mathfrak{D}(\omega-\frac{1}{2}\nu_\mu+\frac{1}{2}\nu_\rho-\nu_\sigma)$	Doppler limit
$+\ -\ -\ +$ / $-\ +\ +\ -$: 0	Doppler limit
$+\ +\ +\ +$ / $-\ -\ -\ -$: $\vartheta^{\text{uni-ho}}$	Homogeneously broadened limit
$+\ +\ -\ -$ / $-\ -\ +\ +$: $\vartheta^{\text{uni-ho}}[\mathfrak{N}_{2(\rho-\sigma)}\sqrt{\bar{N}}$	Homogeneously broadened limit
$+\ -\ -\ +$ / $-\ +\ +\ -$: $\vartheta^{\text{uni-ho}}[\mathfrak{N}_{2(\rho-\mu)}\sqrt{\bar{N}}$	Homogeneously broadened limit

There are 2^N possible steady-state solutions ($\dot{I}_n = 0$ for all n) for the N-mode case, since each I_n can be zero or nonzero independent of the other modes. The solutions are

$$I_n^{(s)} = 0, \quad n \in \mathfrak{Z}$$
$$I_n^{(s)} = \sum_m (\theta^{-1})_{nm} I_m, \quad n, m \in \mathfrak{N} \tag{63}$$

where $\mathfrak{Z}$ is the subset of mode indices corresponding to zero intensities and $\mathfrak{N}$ is the subset for nonzero intensities. Here θ^{-1} is the inverse of the truncated θ matrix, which includes saturation terms of nonzero modes only. Both physical ($I_n \geq 0$) and stable solutions are required. These can be found using an analysis of small vibrations about steady state. Two subsidiary stability requirements are found. First, the effective-gain coefficients

$$\alpha_n' = \alpha_n - \sum_m \theta_{nm} I_m^{(s)}, n \in \mathfrak{Z}, m \in \mathfrak{N} \tag{64}$$

must be negative. These coefficients represent the gain of a mode in the presence of other modes. If $\alpha_n > 0$, the intensity of that mode builds up. The second restriction is that the eigenvalues of the matrix with elements $-2I_n^{(s)}\theta_{nm}(n, m \in \mathfrak{N})$ must have negative real parts. Otherwise, the intensity of at least one mode in $\mathfrak{N}$ decreases to zero.

VII. TWO-MODE OPERATION

To illustrate the formalism and the physics represented therein, we consider the two-mode laser. There are no nonzero slowly varying phase angles, so that the algorithm for finding free-run intensities presented in Sec. VI applies equally to all three lasers under consideration. The intensity equations for two modes are given by

$$\dot{I}_i = 2I_i(\alpha_i - \beta_i I_i - \theta_{ij} I_j),$$
$$i, j = 1, 2; \; i \neq j \tag{65}$$

where $\beta_i = \theta_{ii}$, the self-saturation coefficient and θ_{ij} are the cross-saturation coefficients. Clearly, if either α_i is less than zero, the respective mode is below threshold and its intensity must go to zero. If both net-gain coefficients are negative, no oscillation occurs. If only one is positive the solution $I_i = \alpha_i/\beta_i$ is stable for that mode. If both α's are positive we evaluate the subsidiary stability conditions to see which modes oscillate. The stationary-state ($\dot{I}_i = 0$) equations yield

$$I_i^{(s)} = \alpha_i'[\beta_i(1 - C)]^{-1}, \quad i = 1, 2 \tag{66}$$

where the coupling constant $C = \theta_{12}\theta_{21}/(\beta_1\beta_2)$. If $C < 1$, then the self-saturation predominates and we speak of "weak" intermode coupling. If $C > 1$, an unusual occurence, the cross-mode saturation is predominant. This is called "strong" coupling. $C = 1$ is called "neutral" coupling.

TABLE VIII. Conditions for both stationary and stable solutions of two mode intensities. The coefficients are defined as follows: α_i by Table VI, θ_{ij} by (62), α_i' by (64), $\beta_i = \theta_{ii}$, and $C = \theta_{12}\theta_{21}/\beta_1\beta_2$.

I_1	I_2	Conditions for stability
0	0	$\alpha_1 < 0, \; \alpha_2 < 0$
α_1/β_1	0	$\alpha_1 > 0, \; \alpha_2' > 0$ or $\{\alpha_1'$, and $\alpha_2' < 0, \; C > 1\}$
0	α_2/β_2	$\alpha_1' < 0, \; \alpha_2 > 0$
$\frac{\alpha_1'/\beta_1}{1-C}$	$\frac{\alpha_2'/\beta_2}{1-C}$	$C < 1$
I_1	$(\alpha_1 - \beta_1 I_1)/\theta_{12}$	$C = 1, \; 0 \leq I_1 \leq \alpha_1/\beta_1$

The stability criterion to be considered requires that the eigenvalues of the matrix $-2I_n^{(s)}\theta_{nm}$ must be negative. For both modes 1 and $2 \in \mathfrak{N}$ the matrix has eigenvalues

$$\lambda_{1,2} = -(\alpha_1' + \alpha_2')/(1 - C) \pm \{(\alpha_1' + \alpha_2')^2/(1 - C)^2 - 4\alpha_1'\alpha_2'/(1 - C)\}^{1/2}. \tag{67}$$

If both α_1' and α_2' are greater than zero and $C < 1$, the real parts of both eigenvalues are negative, since the magnitude of the square root is less than that of the leading term. Then (66) represents a stable solution. However, if $C > 1$ and both α's are negative, one value of λ must be positive, so both modes cannot oscillate simultaneously. Since both effective-gain coefficients are negative, each single-mode solution is independently stable with value $I_i = \alpha_i/\beta_i$, while the other mode has zero intensity. The initial conditions determine which mode oscillates, as illustrated by Lamb.[1] We term this condition "bistable operation." If, with $C > 1$, either α' is positive, the fundamental restriction $I_i \geq 0$ is violated for that mode. The same is true for $C < 1$ when either α' negative. The solutions for the two-mode free-run analysis are summarized in Table VIII.

To illustrate the formalism and physical mechanisms we consider the two-mode bidirectional- (one mode traveling in either direction) ring laser, the two-mode unidirectional- (both modes in same direction) ring laser and the two-mode standing-wave (two-mirror) laser. Inasmuch as the last of these consists of four running waves with specific degeneracies yielding the two standing waves, it is the most complicated. In fact, the special case of the two-mode bidirectional-ring which reduces to a single standing wave reveals the nature of interactions responsible for the Lamb dip. To simplify the analytic aspects of our discussion, we take the Doppler limit of Eq. (41) in evaluating

the saturation coefficients in Table VI.

For the bidirectional ring, the two modes E_1 and E_2 coincide with the +1 and −1 in Table V. For higher-mode operation, all modes in the same direction correspond to one of these. Furthermore in the Doppler limit, only the T_{ij} integrals are nonzero with values given by (41) in conjunction with the complex frequencies of Table I. Reading through Table V, we find that the complex self-saturation coefficient ϑ_{++++} contains the nonvanishing integrals T_{21} and T_{31} which have constant values yielding the imaginary part $\beta_+(\beta_1)$ given in Table IX. Similarly, the other running wave has the same value from T_{21} and T_{31} integrals. The cross-saturation coefficient θ_{12} is given by the imaginary part of $\vartheta_{1122}+\vartheta_{1221}$. The first of these ($\vartheta_{1122}$) is given in Table V by T_{11} and T_{41} integrals. It is due to hole burning, for the final subscripts are equal (2), indicating a reduction in population difference due to atomic transitions induced by mode 2. The second complex coefficient ϑ_{1221} results from population pulsations (the final two subscripts are different) and vanishes in the Doppler limit. This can be understood physically, for the pulsation terms arising from atoms moving with axial velocity v contain an exponential factor $\exp(2iKv)$ due to the opposite Doppler shifts encountered for waves running in opposite directions. The total contribution comes from the sum of all velocity groups, that is, from an integral over v. This integral vanishes in the Doppler limit due to the cancellations introduced by the exponential factor. For slower moving media this cancellation is less complete, and for nonmoving media the population pulsations can play an important role, as an analysis of our equations in that limit reveals. The values for θ_{12} and θ_{21} are the same and are given in Table IX. For both the self- and cross-saturation coefficients, we have taken the same cavity Q's. The frequency $\nu_0=\frac{1}{2}(\nu_1+\nu_2)$.

TABLE IX. Two-mode self- and cross-saturation coefficients appearing in Eq. (65).

Coefficients	Physical meaning
Bidirectional-ring	
$\beta_1=\beta_2=\beta=\frac{1}{2}\nu\mathfrak{N}\gamma_{ab}/(Q\gamma)$	self-saturation
$\theta_{12}=\theta_{21}=\theta=\beta\mathfrak{L}(\omega-\nu_0)$	cross saturation, $\nu_0=\frac{1}{2}(\nu_1+\nu_2)$
Unidirectional-ring	
$\beta_1=\beta_2=\beta=\frac{1}{2}\nu\mathfrak{N}\gamma_{ab}/(Q\gamma)$	self-saturation
$\theta_{12}=\theta_{21}=\beta\mathfrak{L}(\Delta/2)\gamma_b$ $\times[1+(\gamma\gamma_a-\frac{1}{2}\Delta^2)(\gamma\gamma_a)^{-1}\mathfrak{L}_a(\Delta)]$ $+\gamma_a\longleftrightarrow\gamma_b$	cross saturation
Standing-wave (two-mirror)	
$\beta_n=\frac{1}{4}\nu\mathfrak{N}\gamma_{ab}(Q\gamma)^{-1}[1+\mathfrak{L}(\omega-\nu_n)]$	self-saturation
$\theta_{12}=\theta_{21}=\theta=\beta+\{\nu\mathfrak{N}\gamma_b(16\gamma Q)^{-1}\mathfrak{L}(\frac{1}{2}\Delta)$ $\times\mathfrak{L}_a(\Delta)[1-\Delta^2/(2\gamma_a\gamma)](1+N_2/\bar{N})$ $+\gamma_a\longleftrightarrow\gamma_b\}$	cross saturation for symmetric tuning $(\omega-\nu_n=\pm\frac{1}{2}\Delta)$

The coupling constant C varies with tuning as $\mathfrak{L}^2(\omega-\nu_0)$. The mode coupling is always weak; however, it is much more appreciable near line center. When the modes are symmetrically placed about line center, $C=1$ and neutral coupling exists. Figure 5 shows a particular solution for the bidirectional laser. The increasing intermode saturation comes from the hole-burning terms, and the intensity dip near central tuning is similar to the Lamb dip of a single-mode standing-wave laser. Specifically, the overlap of the atomic velocity components when tuning is within a homogeneous linewidth of line center reduces the number of atoms available for interaction with the field. At the symmetric tuning point, one of the modes may completely quench the other.

We next investigate the two-mode unidirectional-ring laser. The self-saturation (Table IX) is the same as that for the bidirectional ring, as one would expect. However, the cross-saturation coefficients θ_{12} and θ_{21} differ from the bidirectional case. The leading term on the right-hand side is the hole-burning contribution, while the second term arises from population pulsations in the medium. In this case the pulsations do not contain an integral over the factor e^{2iKv}, since both waves are Doppler shifted with the same sign. Note that

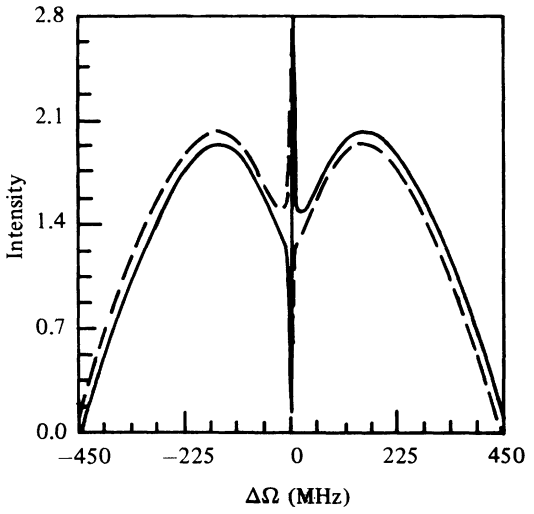

FIG. 5. Two-mode bidirectional-ring intensities vs average cavity detuning. The parameters $\gamma_a=15.5$ MHz, $\gamma_b=41$ MHz, $\gamma=80$ MHz, $Ku=1010$ MHz, $\mathfrak{N}=1.2$, $L=\frac{1}{3}$ m, and the frequency splitting Δ is 15 MHz. Solid curve depicts wave running along increasing s; dashed curve along decreasing s.

there is no special dependence on the location of atomic line center. Here we have a situation where the velocity ensembles of the medium which interact with the two modes can never overlap. The coupling constant is always less than 1. If the laser is short enough so that only two longitudinal modes are supported, the intermode spacing Δ is large and $[\pounds(\frac{1}{2}\Delta)]^2 \approx 0.005$. With almost no cross coupling, the relative intensities of a two-mode unidirectional ring (Fig. 6) are essentially proportional to the atomic gain profile.

Finally, we examine the two-mode standing-wave laser. Here we assume symmetrical tuning about the inhomogeneous line center, $\nu_2 - \omega = \omega - \nu_1 = \frac{1}{2}\Delta$. The self-saturation ($\beta$) terms contain the constant encountered in those of the bidirectional ring plus the Lorentzians appearing in the ring's θ's. This is due to the presence of two oppositely directed running waves in a single standing-wave mode, and the Lorentzian (here producing the Lamb dip) is seen to be due to the saturation by one running wave on the gain of the other wave. This cross saturation is greatest at line center where the velocity ensembles contributing to both running waves coincide. This conclusion was given earlier by Bennett based on a phenomenological hole-burning model.

Since a standing-wave mode interacts strongly with two velocity ensembles, the coupling with a second mode is strongest when the two modes are symmetrically tuned, for it is here that maximum competition for the same velocity groups occurs.

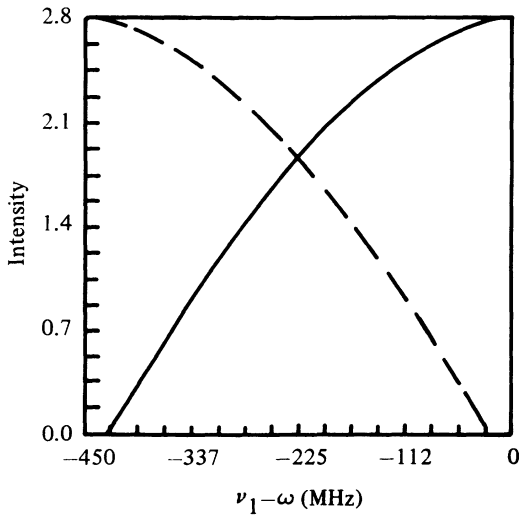

FIG. 6. Two-mode unidirectional-ring intensities vs cavity detuning of the first mode. The parameters are the same as Fig. 5, except there is no cavity rotation. Detuning values of the higher-frequency (second) mode are given by the abscissa plus the cavity mode separation of 450 MHz.

If only hole-burning effects are considered, the cross saturation just equals the self-saturation (the bracketed expression in the θ comes from the population pulsation terms). Although the population pulsation contribution is smaller than the hole-burning terms by about γ/Δ, they can give rise to cases of strong coupling, and hence bistable operation.

Under normal conditions for two-mode oscillation, the cavity is fairly short, corresponding to a fairly large intermode separation Δ. Also, uniform excitation of the laser medium assures $|N_2| \approx 0 < \bar{N}$. Therefore the population pulsation contribution is negative and the coupling is weak. However, if a long laser is operated at low enough excitation so that only two modes are above threshold, it is possible that $2\gamma\gamma_a > \Delta^2$, and strong coupling ($C > 1$) results. Figure 7 is a plot of C as a function of intermode separation, which illustrates the transition to strong coupling. Another consideration, mentioned by Lamb,[1] is a variable excitation density. If $N(z, t)$ is positive in the center of the cavity, but negative in the end quarters, $N_2 < -\bar{N}$ and again $\theta > \beta$.

Figure 8 shows relative intensities versus cavity detuning for a two-mode standing-wave laser with $C < 1$. The coupling is strongest in the midtuning region, where both frequencies compete for the same velocity ensembles. The mode competition results in a rapid intensity crossover at midtuning, where the mode closest to line center dominates. The dominant mode actually quenches the other mode for some values of detuning. At

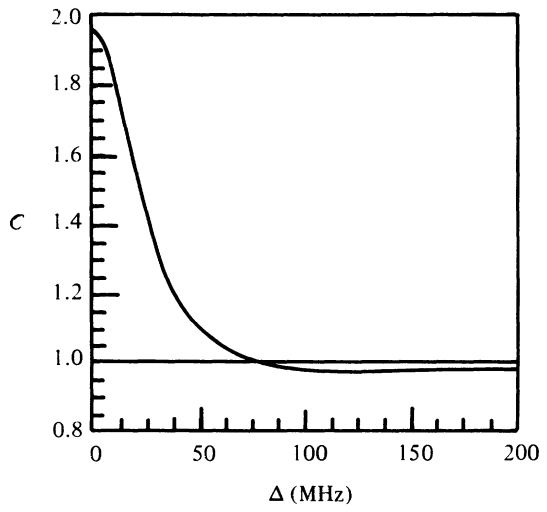

FIG. 7. Two-mode coupling constant vs intermode separation frequency, in the strong Doppler limit. The parameters $\gamma = 100$ MHz, $\gamma_a = 15.5$ MHz, $\gamma_b = 41$ MHz, $N_2/N = -0.25$. Strong coupling can occur for lasers longer than 2 m.

the edges of the plot one or the other mode is tuned to line center and experiences a Lamb dip due to its increased self-saturation.

VIII. MULTIMODE RESULTS

This section is devoted to the discussion of specific examples of many-mode operation. Steady-state solutions of (62) are presented as functions of various parameters, primarily cavity detuning. These mode intensities can be interpreted using the physical mechanisms discussed in previous sections. Whenever possible, the theoretical results are compared to laboratory experiments.

The stable intensities of a four-mode bidirectional-ring laser are shown in Fig. 9. The oppositely directed traveling waves have been frequency split by 15 MHz. The features of this solution are quite reminiscent of the two-mode standing-wave result (Fig. 8), as might be expected. However, near the edges of the plot, only two traveling waves are above threshold, and the traveling wave nearest line center dominates. The frequency splitting leads to significant intensity differences of oppositely directed modes far from line center. If nonreciprocal transmission losses and frequency splitting are absent, the traveling waves of the same frequency have equal intensities. If the polarization decay constant γ is increased, thus increasing the competition for available atoms, one set of traveling waves can be extinguished altogether, as in Fig. 10.

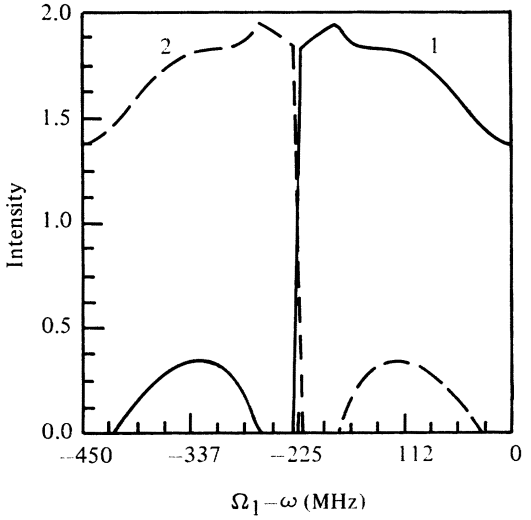

FIG. 8. Two-mode standing-wave intensities vs detuning of the first mode. Corresponding detuning values of the second mode are given by the abscissa plus the intermode spacing of 450 MHz. The parameters $\gamma=2\pi\times128$ MHz, $\gamma_a=2\pi\times15.5$ MHz, $\gamma_b=2\pi\times41$ MHz, $Ku=2\pi\times1010$ MHz, $\mathfrak{N}=1.2$ and $L=0.3333$ m.

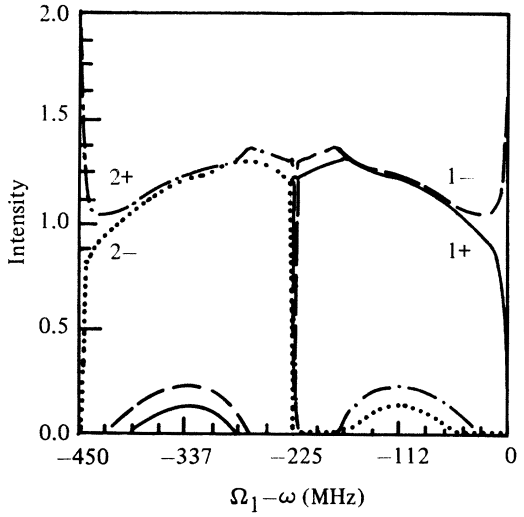

FIG. 9. Four-mode bidirectional-ring laser (two running waves in each direction). The parameters are $\gamma_a=15.5$ MHz, $\gamma_b=41$ MHz, $Ku=1010.0$ MHz, $L=\frac{1}{3}$ m. The solid and dashed curves are for positive and negative running waves of approximately equal frequency, and the dashed-dotted and dotted curves are corresponding waves for a higher cavity frequency. Abscissa value is the average detuning of the first two waves. The corresponding average detuning for the higher-frequency pair is given by the abscissa +450 MHz. Compare this figure with Figs. 5 and 8.

Another example of steady-state intensities in a bidirectional ring is considered in Figs. 11 and 12. Here we present the solutions of positive and negative traveling waves, respectively, for the six-mode case. Here there are regions of strong mode coupling near symmetric tuning which exhibit bistable operation. For the ring laser, re-

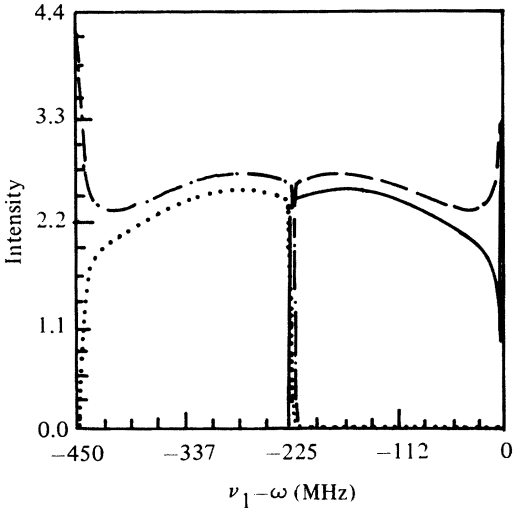

FIG. 10. Four-mode bidirectional-ring laser. Same as Fig. 9 except that γ is increased to 128 MHz.

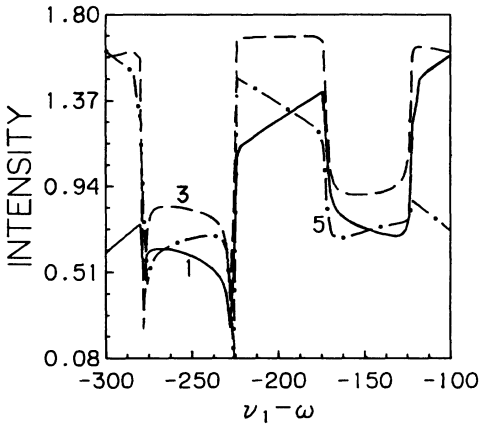

FIG. 11. Six-mode bidirectional ring laser. Intensities of positive running waves vs average detuning of the lowest frequency modes (1 and 2). Other parameters as in Fig. 9. Solid line: mode 1; dashed line: mode 3; dot-dashed line: mode 5. Bistable (unidirectional) region is indicated by vertical lines below detuning axis. Pattern repeats in 200-MHz intervals. Average detuning values for modes 3, 4, and (5, 6) are given by the abscissa value plus the mode separation of 200 MHz (400 MHz).

call that pairs of modes have similar frequencies, which are spaced from the next pair by the longitudinal mode separation. Thus when the central pair of the six-mode ring is symmetrically tuned, there is a large amount of mode competition. Modes 3 and 4 see essentially the same velocity ensemble, and are strongly coupled, as we saw in the two-mode laser (Fig. 8). Further, modes 1, 6 and 2, 5 are symmetrically tuned, and since they are also traveling in opposite directions they compete strongly for the same atoms. This degree of coupling between all sets of modes brings about bistable operation, where the laser becomes unidirectional over a significant detuning range. In the single solution of Figs. 11 and 12, we show the

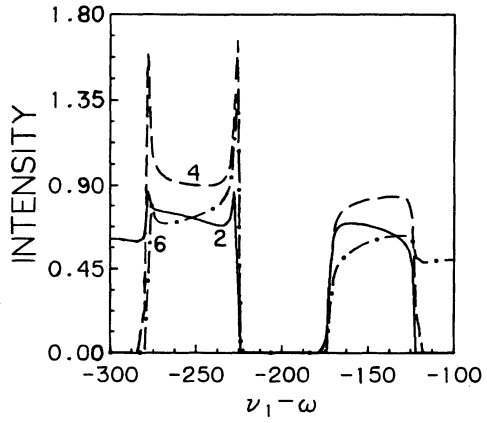

FIG. 12. Six-mode bidirectional ring laser. As in Fig. 11 but for negative running waves. Solid line: mode 2; dashed line: mode 4; and dashed-dotted line: mode 6.

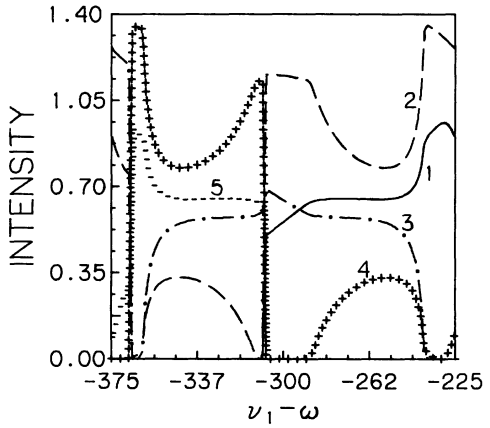

FIG. 13. Intensities of five-mode standing-wave (two-mirror) laser vs detuning of first mode (lowest frequency). Other parameters as in Fig. 8. Detuning values of other modes are given by the abscissa value plus their frequency differences with respect to the first mode.

negative (counterclockwise-traveling) modes nonzero. The other solution is also symmetric but with the positive modes having nonzero intensities. Near the edges of the plot, one pair of modes is detuned away from line center, and the other four modes are again in position to compete for the same velocity components. Again there are two possible solution sets. The detuned modes both oscillate, while the traveling-wave modes in one direction are suppressed. It is interesting to note that the configuration near −300 MHz of Fig. 12 is similar to symmetric tuning of the four-mode ring (−225 MHz in Fig. 9) with the exception of the detuned mode pair. The extra modes contribute additional beat frequency pulsations in the polarization as well as a small constant saturation. This additional coupling increases the saturation of the center two modes unequally, and one of these is suppressed relative to the oppositely traveling wave symmetrical to it. Thus, while the four-mode ring shows a standing-wave character, the six-mode ring shows unidirectional character near points of maximum symmetry.

An example of the solutions of (62) for standing-wave laser operation is given in Figs. 13 and 14. Here we consider a five-mode laser, which exhibits two separate stable solutions in some regions of cavity detuning. Comparison of the figures reveals that whenever modes are symmetrically placed with respect to the atomic line center, the maximum mode competition leads to bistable operation. When the mode locations are not so symmetric under the gain curve, only one stable solution exists. Near central tuning of mode 3 (i.e., $\nu_1 - \omega = -300$ MHz) modes 1, 5 and 2, 4 are symmetrically placed. They experience maximum

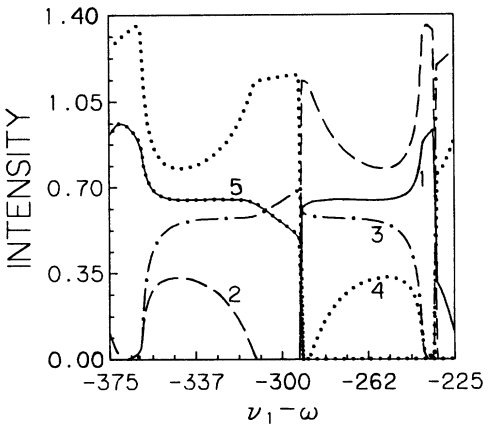

FIG. 14. Five-mode standing-wave laser. As in Fig. 13, but other solution of bistable pair.

competition for the same atomic velocity ensembles, and the intensities cross over rapidly, similar to the cross over in Fig. 8 for two-mode coupling. The actual cross over point is offset from the exact symmetry position in cases of bistable operation. The detuning regions having two solutions occur between points of rapid crossover. The other regions where two solutions exist are located near the edge of the plots. On the left side, modes 2, 5 and 3, 4 are paired symmetrically to the gain curve, while on the right modes 1, 4 and 2, 3 are similarly paired.

The onset of strong coupling occurs at the symmetric tuning point, and the bistable region spreads outward in both directions as the contribution of the population pulsation terms is increased by decreasing the intermode spacing frequency. In this connection, we note that the bi-

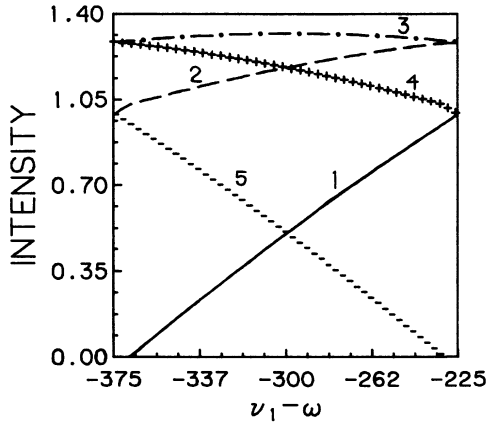

FIG. 15. Intensities of five-mode unidirectional ring laser vs detuning of first (lowest-frequency) mode. Detuning values of other modes are given by the abscissa value plus their frequency differences with respect to mode 1.

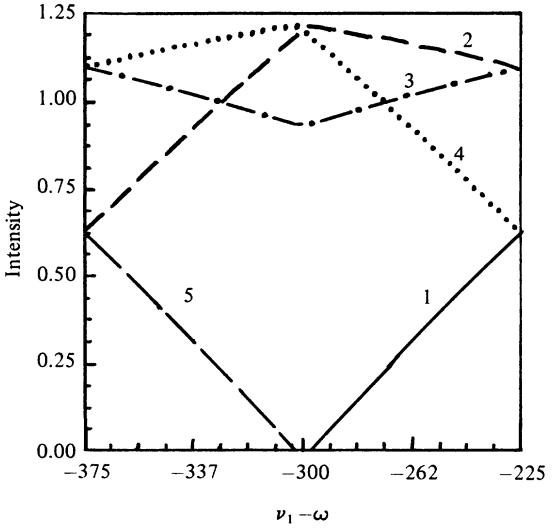

FIG. 16. Five mode unidirectional ring laser. Same as Fig. 15 but with $\gamma = 128$ MHz.

stability vanishes here as for the two-mode case (Fig. 8) when population pulsations (artificially) are dropped. It also disappears in the unidirectional-ring laser, where each mode sees essentially a single velocity group instead of the symmetrically placed pair contributing to standing wave modes. This fact is illustrated in Figs. 15 and 16 for unidirectional-ring operation. In Figs. 17 and 18 ten-mode standing-wave operation characteristics are shown.

Note that at central tuning for the middle mode the mode spectrum is asymmetrical such that modes oscillate either above or below line center. Asymmetrical operation has been reported by

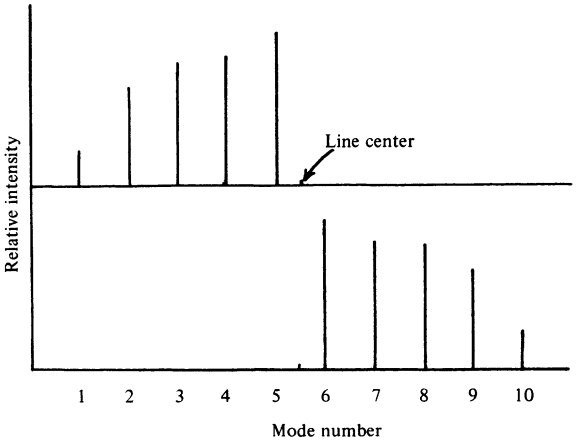

FIG. 17. Diagram depicting mode placement in ten-mode standing-wave bistable operation. Modes oscillate on either side of line center, but not on both. The corresponding unidirectional laser has a single symmetric solution.

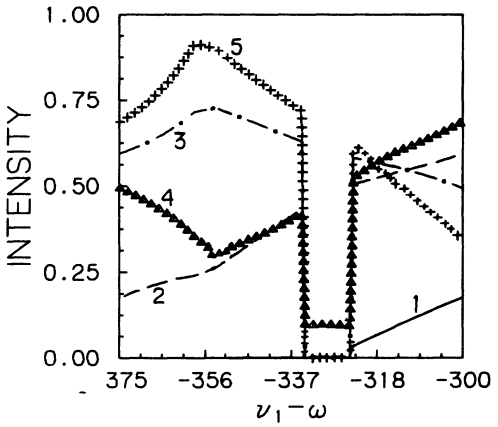

FIG. 18. Ten-mode free-run standing wave. Intensities vs detuning—first of two stable solutions, with oscillating mode on dc side of line center. Figure 17 shows relationship of this solution to the other stable solution.

Garside,[14] who notes that for a free-running He Ne laser, the spectrum is dominant on the low-frequency side. Garside suggests that the transverse character of the mode leads to focusing of the beam below line center and defocusing above. This results in slightly different cavity Q's for different modes. The focused modes have higher Q's, leading to the observed operation on the low-frequency side. Figure 17 shows the two bistable solutions of the ten-mode standing-wave laser at central tuning. By increasing the relative Q for the low-frequency modes by 1%, the high-frequency bistable solution is extinguished, but the resultant mode spectrum retains the asymmetric form of Fig. 18.

ACKNOWLEDGMENTS

The author would like to thank A. G. Fox, W. E. Lamb, Jr., and D. R. Hanson for stimulating conversations.

APPENDIX: PLASMA DISPERSION FUNCTION AND ITS THIRD-ORDER GENERALIZATION

The plasma dispersion function is historically defined[20] as

$$Z(\zeta) = \pi^{-1/2} \int_{-\infty}^{\infty} dx\, e^{-x^2}/(x-\zeta) \tag{A1}$$

valid for $\mathrm{Im}\zeta > 0$, and the analytic continuation of this for $\mathrm{Im}\zeta < 0$. If ζ is wholly real, $Z(\zeta)$ is the Hilbert transform of the Gaussian. Another expression for $Z(\zeta)$ is related to the error function:

$$\begin{aligned} Z(\zeta) &= 2ie^{-\zeta^2} \int_{-\infty}^{i\zeta} e^{-t^2}\, dt \\ &= i\pi^{1/2} e^{-\zeta^2} [1 + \mathrm{erf}(i\zeta)]. \end{aligned} \tag{A2}$$

In the present theory, we derive the double integral

$$iK\pi^{-1/2} \int_0^{\infty} d\tau' \int_{\infty}^{\infty} dv\, e^{-(v/u)^2} e^{-(v+iKv)\tau'} \tag{A3}$$

which we call the plasma dispersion function also. When the integral over τ' is evaluated first, the result is similar to (1),

$$Z(v) = iK\pi^{-1/2} \int_{-\infty}^{\infty} dv\, e^{-(v/u)^2} (v + iKv)^{-1}. \tag{A4}$$

We note that these definitions are identical if $\zeta = iv/Ku$. However, we find it convenient to denote (3) and (4) by $Z(v)$, which has an argument with dimensions of frequency. The integral over v can be evaluated first, leading to yet another form of the dispersion function

$$Z(v) = iKu \int_0^{\infty} d\tau' \exp[-v\tau' - \tfrac{1}{4}(Ku)^2 \tau'^2]. \tag{A5}$$

In evaluation of coefficients in the third-order theory, it is useful to know the following symmetry properties:

$$\begin{aligned} &Z(-v) = -Z(v), \\ &Z(v^*) = -[Z(v)]^*. \end{aligned} \tag{A6}$$

Several limiting cases are of interest. If there is no atomic motion,

$$Z(v)_{u \to 0} = iKuv^{-1}. \tag{A7}$$

When the Doppler width Ku is much larger than the homogeneous broadening width γ, that is, in the "Doppler limit,"

$$\begin{aligned} Z(i\Delta\omega)_{(Ku \gg \gamma)} = {} & i\pi^{1/2} e^{-[\Delta\omega/(Ku)]^2} \\ & - 2\, e^{-(\Delta\omega/Ku)^2} \int_0^{\Delta\omega/Ku} dx\, e^{x^2}. \end{aligned} \tag{A8}$$

Finally, if the radiation is on resonance with the atomic medium, v is wholly real, and

$$Z(\gamma) = i\pi^{1/2} e^{(\gamma/Ku)^2} \{1 - \mathrm{erf}(\gamma/Ku)\}. \tag{A9}$$

In the third-order perturbation terms, there appear three time integrals in addition to the velocity integral. These integrals form a natural extension of the plasma dispersion function, with three complex frequencies v_1, v_2, and v_3, and three wave numbers K_1, K_2, K_3. Here we assume that the wave numbers are the constant multiples c_1K, c_2K, and c_3K. Then by simply writing $Z(v)$ as (3) and tripling the integral on τ, we arrive at the third-order integral

$$\begin{aligned} T = {} & iK\pi^{-1/2} \int dv \exp[-(v/u)^2] \int d\tau' \int d\tau'' \int d\tau''' \\ & \times \exp\{-[(v_1 + ic_1Kv)\tau' + (v_2 + ic_2Kv)\tau'' + (v_3 + ic_3Kv)\tau''']\}. \end{aligned} \tag{A10}$$

It is possible to express T in terms of $Z(v)$ by completing the square in v and then suitably transforming variables. This method was used in Sargent, Lamb, and Fork.[2] However, it is simpler as well as more general to integrate the time variables first and use partial fractions to expand the resulting integrand. Thus

$$T = iK\pi^{1/2} \int_{-\infty}^{\infty} dv\, e^{-(v/u)^2} \times [(v_1 + ic_1Kv)(v_2 + ic_2Kv)(v_3 + ic_3Kv)]^{-1}. \quad \text{(A11)}$$

and the denominator can be expanded to

$$\left(\frac{1}{c_1v_2 - c_2v_1}\right)\left(\frac{c_1}{v_1 + ic_1Kv} - \frac{c_2}{v_2 + ic_2Kv}\right)\left(\frac{1}{v_3 + ic_3Kv}\right)$$
$$= \left(\frac{1}{c_1v_2 - c_2v_1}\right)\left[\left(\frac{c_1}{c_1v_3 - c_3v_1}\right)\left(\frac{c_1}{v_1 + ic_1Kv} - \frac{c_3}{v_3 + ic_3Kv}\right) - \left(\frac{c_2}{c_2v_3 - c_3v_2}\right)\left(\frac{c_2}{v_2 + ic_2Kv} - \frac{c_3}{v_3 + ic_3Kv}\right)\right]. \quad \text{(A12)}$$

Using (A4) for $Z(v)$, along with (A11) and (A12), we find

$$T_{tw} = \left(\frac{1}{c_2v_1 - c_1v_2}\right)\left(c_1\frac{Z(v_3/c_3) - Z(v_1/c_1)}{c_1v_3 - c_3v_1} - c_2\frac{Z(v_3/c_3) - Z(v_2/c_2)}{c_2v_3 - c_3v_2}\right). \quad \text{(A13)}$$

In the laser theory, the three complex frequencies depend on which particular branch t of the perturbation tree is under consideration. The values of the v_{tk} are given in Table I. Likewise, the constants c_k depend on the direction of the interaction components, or the index w. Table II summarizes the values of c_{wk} required. Using these values, we find the particular cases of T_{tw}:

$$T_{t1} = [1/v_{t2}][Z(v_{t1}) + Z(v_{t3})]/(v_{t1} + v_{t3}), \quad \text{(A14)}$$

$$T_{t2} = -[1/v_{t2}][Z(v_{t1}) - Z(v_{t3})]/(v_{t1} - v_{t3}), \quad \text{(A15)}$$

and

$$T_{t3} = \frac{1}{2}\frac{1}{v_{t1} - v_{t2}/2}\left(\frac{Z(v_{t3}) - Z(v_{t1})}{v_{t3} - v_{t1}} - \frac{Z(v_{t3}) - Z(\frac{1}{2}v)_{t2}}{v_{t3} - \frac{1}{2}v_{t2}}\right). \quad \text{(A16)}$$

It is not uncommon for v_{t1} to equal v_{t3}. If this occurs, we can use

$$\lim_{v_{t3} \to v_{t1}} [Z(v_{t3}) - Z(v_{t1})]/(v_{t3} - v_{t1}) = dZ(v_{t1})/dv_{t1} \quad \text{(A17)}$$

in T_{t2} and T_{t3}.

For stationary atoms, $Z(v)$ is given by (A7) and

$$T_{tw} \xrightarrow[u \to 0]{} iKu/v_{t1}v_{t2}v_{t3}. \quad \text{(A18)}$$

An assumption often used to write results for the third-order complex polarization is the "strong Doppler limit." In this approximation all frequency intervals $\omega - \nu$, $2\nu_2 - \nu_1$, etc., are assumed much smaller than the Doppler with Ku. The homogeneous decay constants γ, γ_a, and γ_b are also much less than Ku.

Then

$$Z(v) \xrightarrow[Ku \gg \gamma, \Delta\omega]{} i\pi^{1/2}.$$

In this stringent but often applicable limit, the third-order integrals become

$$T_{t1} \approx 2i\pi^{1/2}[v_{t2}(v_{t1} + v_{t3})]^{-1}, \quad T_{t2} \approx T_{t3} \approx 0. \quad \text{(A19)}$$

*Work supported in part by the Air Force Weapons Laboratory, Kirtland Air Force Base, N. M. Work of M. Sargent also supported in part by Bell Telephone Laboratories, Holmdel, N. J.

†Current address: Space and Missile Systems Organization, Los Angeles, Calif.

[1]W. E. Lamb, Jr., Phys. Rev. 134, A1429 (1964).

[2]W. R. Bennett, Jr., App. Opt. Suppl. 1, 24 (1962). See also his contribution in *Proceedings of the Brandeis 1969 Summer Institute of Theoretical Physics* (Gordon and Breach, New York, 1971).

[3]H. Haken and H. Sauermann, Z. Phys. 173, 261 (1963); Z. Phys. 176, 47 (1963).

[4]F. Aronowitz, Phys. Rev. 139, A635 (1965). S. G. Zeigler and E. E. Fradkin, Opt. Spek. 21, 386 (1966) [Opt. Spec. 21, 217 (1966)]; L. Menegozzi and W. E. Lamb, Jr., Phys. Rev. A8, 2103 (1973).

[5]M. Sargent III, R. L. Fork, and W. E. Lamb, Jr., Phys. Rev. 164, 436 (1967); Phys. Rev. 164, 450 (1967).

[6]K. Uehara and K. Shimoda, Jap. J. Appl. Phys. 4, 921 (1965); W. Culshaw, Phys. Rev. 164, 329 (1967).

[7]M. O. Scully and W. E. Lamb, Jr., Phys. Rev. 159, 208 (1967); Phys. Rev. 166, 246 (1968). See also the work of Lax, as summarized in his chapter in the *1966 Brandeis University Summer Institute Lectures*, edited by M. Chretien, E. P. Gross, and S. Deser (Gordon and Breach, New York, 1969); and the work of Haken and co-workers described and referenced in

Laser Theory, Encyclopedia of Physics, Vol. XXV/2c, edited by S. Flügge (Springer-Verlag, Berlin, 1970).

[8]P. R. Berman and W. E. Lamb, Jr., Phys. Rev. A 2, 2435 (1970); Phys. Rev. A 4, 319 (1971). See also S. G. Rautian, Zh. Eksp. Teor. Fiz. 51, 1176 (1966) [Soviet Phys.—JETP 24, 788 (1967)]; B. L. Gyorffy, M. Borenstein, and W. E. Lamb, Jr., Phys. Rev. 169, 340 (1968).

[9]S. Stenholm and W. E. Lamb, Jr., Phys. Rev. 181, 618 (1969); B. J. Feldman and M. S. Feld, Phys. Rev. A 1, 1375 (1970).

[10]L. Menegozzi and W. E. Lamb, Jr., Ref. 4.

[11]M. Sargent and M. O. Scully, *Laser Handbook,* edited by F. T. Arecchi and E. O. Schultz-DuBois (North-Holland, Amsterdam, 1972), Chap. A2. See also H. Haken's chapter (A3) in this book, and M. Sargent III, M. O. Scully, and W. E. Lamb, Jr., *Laser Physics* (Addison-Wesley, Reading, Mass., 1974).

[12]M. O. Sayers and L. Allen, Phys. Rev. A 1, 1730 (1970).

[13]A somewhat more general calculation on the multimode Zeeman ring laser has been made by D. R. Hanson and M. Sargent, III, Phys. Rev. A (to be published). The increased generality tends to obscure the purely scalar multimode theory given here.

[14]B. K. Garside, IEEE J. Quantum Electronics QE-4, 940 (1968).

[15]P. W. Smith, Proc. IEEE 58, 1342 (1970). See also P. W. Smith, M. Duguay and E. P. Ippen, *Mode Locking of Lasers* (Pergamon, New York, 1973).

[16]P. H. Lee and J. G. Atwood, IEEE J. Quantum Electronics QE-2, 235 (1966).

[17]D. H. Close, Phys. Rev. 153, 360 (1967).

[18]C. Whitney, Phys. Rev. 191, 535 (1969).

[19]T. Miyoshita, H. Mori, and J. Ikenoue, Jap. J. Appl. Phys. 10, 1051 (1971).

[20]B. D. Fried and S. D. Conte, *The Plasma Dispersion Function (Hilbert Transform of the Gaussian)* (Academic, New York, 1961).